IEEE Access
Multidisciplinary ⋮ Rapid Review ⋮ Open Access Journal

Received 3 December 2024, accepted 19 December 2024, date of publication 26 December 2024, date of current version 6 January 2025.

Digital Object Identifier 10.1109/ACCESS.2024.3522291

RESEARCH ARTICLE

Coordinated Design of Power System Stabilizer and Virtual Inertia Control Using Modified Harris Hawk Optimization for Improving Power System Stability

MOHAMAD ALMAS PRAKASA[1], IMAM ROBANDI[1], ALBERTO BORGHETTI[2], MUHAMMAD RUSWANDI DJALAL[1], AND WASEDA HIMAWARI[1]

[1]Department of Electrical Engineering, Institut Teknologi Sepuluh Nopember, Surabaya 60111, Indonesia
[2]Department of Electrical, Electronic and Information Engineering, University of Bologna, 40136 Bologna, Italy

Corresponding author: Imam Robandi (imam.robandi@its.ac.id)

This work was supported by the Directorate of Research and Community Service (Direktorat Riset, Teknologi, dan Pengabdian kepada Masyarakat–DRPM), Ministry of Education, Culture, Research, and Technology (Kementerian Pendidikan, Kebudayaan, Riset dan Teknologi–Kemendikbudristek) of the Republic of Indonesia under Grant 1760/PKS/ITS/2024.

ABSTRACT In the current era, power system stability faces typical problems due to the Renewable Energy Sources (RES) integration trend. This trend makes the coordination between power system controllers crucial to maintain stability across a wide-range of operating behaviors. To address this problem, this paper proposes the coordinated design of Power System Stabilizer and Virtual Inertia Control (PSS-VIC) to improve the stability of the power system integrated with RES. The proposed method uses the modified version of Harris Hawk Optimization with Memory Saving Strategy (HHO-MSS) to find the equilibrium point of global parameters of PSS-VIC through various simulations to ensure scalability. In this proposed method, PSS is focused on increasing the power system stability from the traditional generator sides with diesel engines, thermal, and hydro turbines. Meanwhile, the modified VIC design is proposed to increase the power system stability from the RES sides using virtual inertia emulation with the integration of wind generators, solar photovoltaic units, and energy storage systems. The global parameters of PSS-VIC are determined by calculating the optimal damping ratio which is permitted by grid codes alongside various stability criteria validation. Based on the obtained results, HHO-MSS is 1.44% to 9.28% more accurate and 34.63% to 53.94% more consistent than Electric Eel Foraging Optimization (EEFO), and Puma Optimizer (PO), Evolutionary Mating Algorithm (EMA). With the optimal damping ratios of 9.94% to 9.96% achieved by HHO-MSS, the overall power system stability improvements, including both local and interarea responses across 38 simulations involving sudden load changes, varying inertia, and different RES levels, are as follows: 41.17% to 70.89% frequency nadir improvement, 25.9% to 67.38% power angle deviation improvement, 84.83% to 85.26% settling time reduction, and 51.57% to 89.73% average error reduction calculated with performance indices. The proposed coordinated PSS-VIC design offers excellent scalability and can effectively improve power system stability across a wide-range of operating conditions.

INDEX TERMS Harris hawk optimization, optimal coordinated design, power system stability, power system stabilizer, renewable energy sources, virtual inertia control.

NOMENCLATURE

D	Damping value.
Dim	Dimension of search space of algorithm.
D_{VI}	Tuneable parameter of virtual damping.

The associate editor coordinating the review of this manuscript and approving it for publication was Nagesh Prabhu.

E_{fd} Excitation voltage.
E_o Initial energy of the rabbit of HHO.
E_{ESC} Escaping energy of the rabbit of HHO.
E_q Terminal voltage of the generator.
H Inertia value.
H_{avg} Average vector of the hawks of HHO.
H_p Vector of the hawk of HHO.
H_{pool} Best movement of the hawks.
H_r Vector of random hawk of HHO.
I_t Iteration of algorithm.
J_R Jumping movement of the rabbit of HHO.
k_a Gain constant of amplifier.
K_{PSS} Gain constant of PSS.
K_s Constant of ACE.
K_{VI} Tuneable parameter of virtual inertia.
K_{1-6} Dynamic constant of the electrical part of the generator.
f_{tie} Tie-line frequency.
f Frequency.
lb Lower bound of search space.
LF Levy flight of the rabbit of HHO.
P_c ACE output.
P_e Electrical power.
P_g Governor output.
P_L Load demand.
P_m Power produced by the generator.
P_P Primary control output.
P_{PV} Power generated by PV.
P_{tie} Power flow in tie-line.
P_{VI} Injected virtual inertia emulation.
P_{WG} Power generated by WG.
R Vector of the rabbit of HHO.
r_{ESC} Escape probability of the rabbit of HHO.
R_D Droop constant of turbines.
R_{VI} Droop constant of VIC.
r_{1-5} Random parameter of HHO.
T_a Time response of the amplifier.
T_{ESS} Time response of ESS.
T_e Electrical torque.
T_{exc} Time response of exciter.
T_g Time response of the governor.
T_{INV} Time response of the inverter.
T_m Mechanical torque.
T_T Time response of turbines.
T_{WG} Time response of WG.
T_{WO} Time response of wash-out filter of PSS.
T_{1-4} Tuneable parameter of lead or lag control of PSS.
T_{6-9} Lead or lag control of PSS.
ub Upper bound of search space.
V_{PSS} Stability reference of PSS.
V_t Terminal voltage of area.
V_W Wind speed.
β Bias factor.
δ Power angle.
ζ Damping ratio of the system.
λ Eigenvalue of the system.
Δ Change of variable or deviation of variable.
ω Rotor speed of generator.
Φ Solar irradiance.

LIST OF ABBREVIATION

ACE	Area Control Error.
AGC	Automatic Generation Controller.
AOA	Arithmetic Optimization Algorithm.
AVR	Automatic Voltage Regulator.
DE	Diesel Engine.
EEFO	Electric Eel Foraging Optimization.
EMA	Evolutionary Mating Algorithm.
EOA	Equilibrium Optimizer Algorithm.
ESS	Energy Storage System.
FLC	Fuzzy Logic Controller.
HHO	Harris Hawk Optimization.
HT	Hydro Turbine.
IAE	Integral Absolute Error.
ISE	Integral Squared Error.
ITAE	Integral Time Absolute Error.
ITSE	Integral Time Squared Error.
MFO	Moth Flame Optimization.
MOA	Mayfly Optimization Algorithm.
MSS	Memory Saving Strategy.
PID	Proportional-Integral-Derivative.
PO	Puma Optimizer.
PSS	Power System Stabilizer.
PV	Photovoltaic.
RES	Renewable Energy Source.
RoCoF	Rate of Change of Frequency.
SMIB	Single Machine Infinite Bus.
SSSC	Synchronous Series Compensator.
STATCOM	Static Synchronous Compensator.
SVC	Static VAR Compensator.
TCSC	Thyristor Controlled Series Capacitor.
TP	Tuneable Parameter.
TT	Thermal Turbine.
VIC	Virtual Inertia Control.
WG	Wind Generator.

I. INTRODUCTION

Maintaining the reliability and resilience of power systems has become very challenging due to the rapid development of technology [1], [2]. This development leads to the unique topology and its operating schemes, thus it requires a very specific mitigation method when the power system has problems. One of the crucial problems is the power system stability problems by small disturbances, which have small oscillations and cannot be directly detected [3], [4]. This type of disturbance affects the frequency, voltage, and power responses of both the local and interarea of the power systems. When this disturbance becomes larger, then it can spread from one area to another through interconnection lines

if it is not mitigated quickly and properly. Thus, the power system stability can be compromised.

The power system stability improvement when small disturbances occur is closely related to the dynamic stability approach. This approach may simplify the complex power system into a manageable design that accurately represents its dynamic behavior [5]. The main idea is to add counter-torque by providing damping and inertia properties to dampen the oscillations. In a traditional power system, stability can be maintained by utilizing Load Frequency Control (LFC) and Automatic Voltage Regulator (AVR) loops [6]. LFC loop consists of a speed droop governor, Automatic Generation Control (AGC), and Area Control Error (ACE). While the AVR loop consists of the excitation system. In addition, a Power System Stabilizer (PSS) is very important to improve the power system stability limit through the AVR loop [7], [8].

The PSS is widely used in both traditional and modern power systems because its performance can be easily adjusted. The performance of the PSS in improving power system stability depends on specific parameters that need to be optimally tuned. To increase the stability effects, the PSS design is combined with the other stability controllers, such as in [9], which discusses the coordinated PSS design with Automatic LFC and AVR. In [10], the Thyristor Controlled Series Capacitor (TCSC) is combined with the PSS design. Besides that, the Static Synchronous Compensator (STATCOM) is also combined with PSS design [11], [12], as well as the Static Synchronous Series Compensator (SSSC) which is the series version of STATCOM [13], [14]. In recent studies, PSS design is often combined with a Static VAR Compensator (SVC) to increase the reactive power injection capability of power systems. This combination is explored by using simple models, such as the Heffron-Phillips model for Single Machine Infinite Bus (SMIB) systems [15], [16], and by using more complex models, such as interconnected power systems [17], [18], [19]. Moreover, the PSS-SVC design has been also tested referring to the model of the Sulselrabar Electricity System in Indonesia [20].

Despite the extensive literature on PSS combination with other controllers, it is mostly limited to being effective only in power systems with traditional generators. Along with the increasing integration of Renewable Energy Sources (RES) in modern power systems, this current PSS combination faces problems. Popular RES, such as wind and photovoltaic units, are typically built with power-electronic-based generators that lack damping and inertia properties, making it more challenging to maintain stability. In addition, improper regulation of RES power injection can further disrupt stability. Recently, a hybrid control scheme of PSS and Virtual Inertia Control (VIC) has been proposed [21], [22]. PSS and VIC offer complementary benefits for stability: PSS is effective when traditional generators dominate, while VIC is effective for systems with a high share of RES. With VIC, the power systems can replicate the damping and inertia effects of PSS by regulating the Energy Storage System (ESS) and inverter behavior to inject precisely and timely when the stability is disturbed, as indicated by the declining Rate of Change of Frequency (RoCoF) [23], [24], [25]. This approach replicates the counter-torque effects of damping and inertia properties in synchronous generators, helping to mitigate oscillations caused by small disturbances [21], [22]. Both PSS and VIC rely on parameters that need to be optimally tuned to achieve the best stability effect.

The design of PSS and VIC has developed rapidly. This development includes the use of optimal and adaptive control methods [26], [27]. PSS and VIC designs are also commonly developed using the Fuzzy Logic Controller (FLC) or Proportional-Integral-Derivative (PID), and sometimes through a cooperative approach that combines both [28], [29], [30], [31]. While FLC and PID controllers are easy to implement with PSS, they introduce numerous tuneable parameters, increasing dependency on stochastic factors. Learning-based algorithms, such as machine, deep, and reinforcement learning [32], [33], [34], [35] have also been applied. These algorithms provide useful feedback but rely heavily on dataset availability, making them harder to implement in specific power system models with limited data. As a result, metaheuristic algorithms become popular due to their flexibility and robustness in handling exploration and exploitation processes [7], [36]. These algorithms are very well-suited for optimizing the design of various stability controllers in power systems.

From the literatures, classic and new generations of metaheuristic algorithms are widely used for designing the PSS or VIC [7], [37]. Recent novel metaheuristic algorithms have shown significant improvements, including Equilibrium Optimizer Algorithm (EOA) [38], Arithmetic Optimization Algorithm (AOA) [39], Mayfly Optimization Algorithm (MOA) [20], [40], Harris Hawk Optimization (HHO) [21], [22], [41]. Among the novel algorithms, HHO is gaining popularity due to its unique exploration and exploitation mechanisms, which provide significant scalability for handling various cases. Recently, it has been enhanced with a Memory Saving Strategy (MSS) which outperforms EOA, AOA, and Moth Flame Optimization (MFO) [21], [22]. While HHO-MSS demonstrates significant improvements over the basic HHO, its performance requires further comparison with more recent algorithms to fully evaluate its effectiveness.

Based on the literature, several research gaps remain to be addressed. First, despite the PSS-VIC design carried out in [21] and [22], the optimal parameters vary under different conditions. In addition, the performance of PSS or VIC is typically evaluated under only a single specific disturbance [7], [37]. Moreover, most of the literature does not take respective grid codes or regulations into account to validate the performance of PSS and VIC. In practice, it is necessary to define global parameters for PSS-VIC that are effective across the majority of the power system's operating range to ensure scalability. Second, most existing literature relies on simple optimization methods for stability

controllers. For instance, literature that presents design optimization based on eigenvalue properties often overlooks performance index evaluation, and vice versa [3], [42]. Third, the relationship between RES and VIC performance has been scarcely explored, primarily because the design does not allow for in-depth investigation [23]. To address the research gaps in current trends, this paper proposes the following contributions:

1) A coordinated design of PSS-VIC is proposed to maximize the stability effect of each controller and ensure that their effects do not interfere, which could degrade performance. The global parameters of PSS-VIC are determined by calculating the equilibrium point of the optimal parameters with the improved version of HHO-MSS, which has been evaluated under 38 simulation conditions, including sudden load changes, inertia variations, and varying levels of RES, to demonstrate its scalability in wide-range operating behaviors. The proposed PSS-VIC is tested on a system consisting of a group of synchronous machine interfaced generators, including diesel units, thermal, and hydro turbines, as well as power electronic interfaced RES generators, such as wind and solar photovoltaic.
2) A novel optimization method based on HHO-MSS is proposed by utilizing the damping ratio which permitted by grid codes and incorporating various stability criteria constraints to ensure the quality of the global parameters. Additionally, HHO-MSS performance is compared to newer algorithms, such as the Evolutionary Mating Algorithm (EMA) [43], Electric Eel Foraging Optimization (EEFO) [44], and Puma Optimizer (PO) [45].
3) This paper proposes a specific design of virtual inertia emulation based on the integration of RES, inverters, and ESS, allowing the assessment of the impact of RES availability on virtual inertia emulation effectiveness.

The structure of this paper is the following: Section II presents the design of power systems and stability controllers, including the modified model of VIC. Section III focuses on the formulation of the proposed method for optimizing PSS-VIC design using HHO-MSS to improve power system stability. Section IV explains the proposed simulations to determine the global PSS-VIC parameters by using HHO-MSS and discusses the scalability of the PSS-VIC. Section V summarizes the main findings, outlines the limitations, and explores the prospect of future work.

II. SYSTEM DESIGN

In this paper, the simulation is tested in the power system model as shown in Fig. 1. This system is divided into two areas, which are coupled with a tie-line switch as an interconnection to allow the power transfer from one area to the other. Both areas have similar topologies but differ in parameters that assume the two areas have different capacities. In each area, the generator represents a group of aggregated machines consisting of diesel engines, thermal, and hydro turbines. The traditional generators are connected to LFC and AVR control loops. Additionally, PSS is also connected to the AVR control loop. Meanwhile, Wind Generators (WG) and solar Photovoltaic units (PV) are integrated as power-electronic-interfaced RES generators. The RES components are connected to the ESS, inverters, and VIC to realize the virtual inertia emulation. Each area has its load center to be supplied by the power system.

The power system is modeled using dynamic equations given in Equation (1) and Equation (2). These equations describe the relationship between power exchange and power angle deviation in the tie-line.

$$\Delta P_{tie}(s) = T\,\Delta\delta_{tie}(s) \tag{1}$$

$$\Delta\dot{\delta}_{tie} = \Delta\delta_1 - \Delta\delta_2 \tag{2}$$

with ΔP_{tie} is the amount of power exchanged from one area to the other area, T is the synchronizing coefficient, $\Delta\delta_{tie}$, $\Delta\delta_1$, and $\Delta\delta_2$ are the power angle deviations in tie-line, Area 1, and Area 2, respectively. The relationship between $\Delta\delta$ and Δf in Area 1 and Area 2 is given by Equation (3) and Equation (4), respectively.

$$\Delta\dot{\delta}_1 = \omega_{r1}\Delta f_1 \tag{3}$$

$$\Delta\dot{\delta}_2 = \omega_{r2}\Delta f_2 \tag{4}$$

with ω_r is the rotor speed of the generator with $f = \omega/2\pi$.

The proposed power system stability improvement by PSS-VIC is strongly related to frequency responses. In PSS, Δf or $\Delta\omega$ of the generators is used as the main input to indicate the current state of stability. Meanwhile in VIC, the stability is related to the derivative of Δf, called RoCoF. Δf of each area can be obtained by Equation (5).

$$\Delta\dot{f} = \frac{1}{2H}\left(\Delta P_m - \Delta P_e + \Delta P_{WG} + \Delta P_{PV} + \Delta P_{VI} - \Delta P_L - D\Delta f - T\Delta\delta_1 + T\Delta\delta_2\right) \tag{5}$$

with the dynamic response of the traditional generator represented by the swing equation consisting of H and D as inertia and damping properties, respectively. ΔP_m is the total mechanical power or torque generated. ΔP_{WG} and ΔP_{PV} are the power generated from WG and PV, respectively. ΔP_{VI} is the injected power from virtual inertia emulation. ΔP_L is the load change. ΔP_{tie} is the amount of power exchanged from one area to the other area. 1 and 2 indicate the two areas of the power system.

A. MODEL OF GENERATOR AND PSS

The dynamic model of the generator consists of mechanical parts producing ΔP_m and electrical parts producing ΔP_e. The dynamic models of the mechanical parts of the generators incorporating the LFC control loop are given in Equation (6) until Equation (8).

$$\Delta\dot{P}_m = \frac{1}{T_g}\left(\Delta P_g - \Delta P_m\right) \tag{6}$$

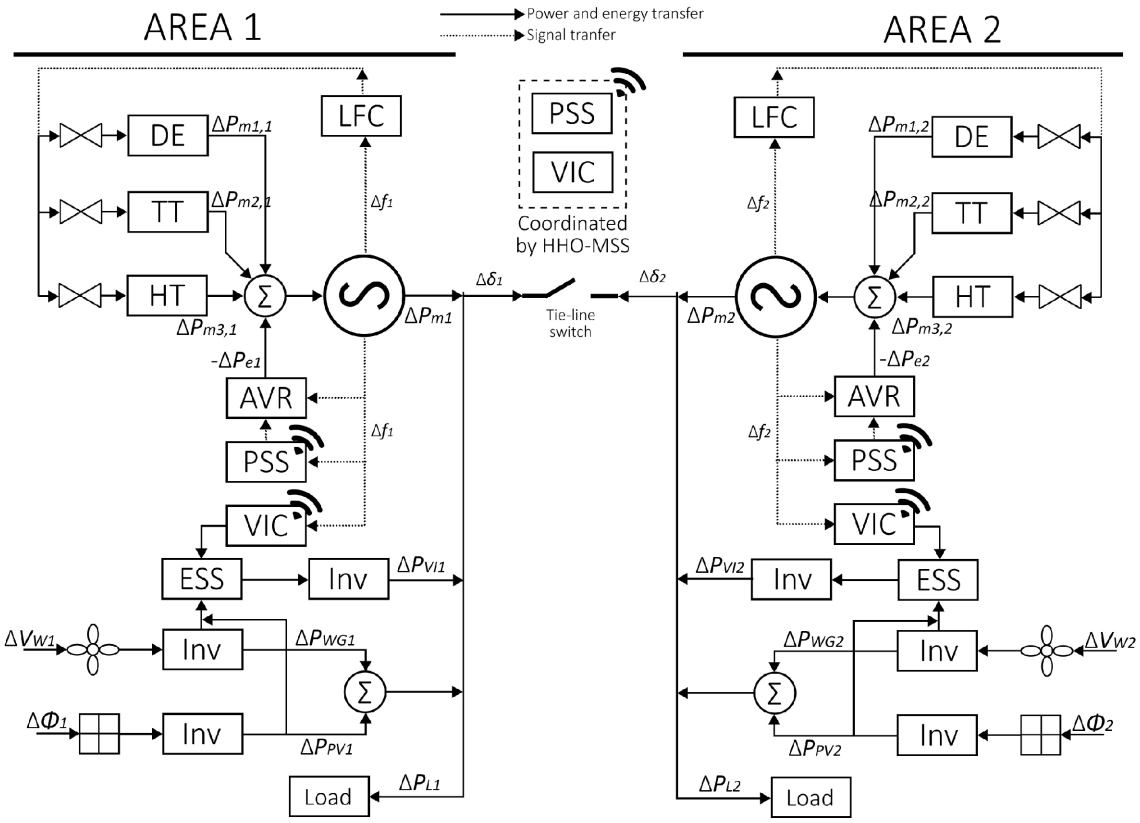

FIGURE 1. Proposed power systems with PSS-VIC design.

$$\Delta\dot{P}_g = \frac{1}{T_T}\left(-\frac{\Delta f}{R_D} - \Delta P_g + \Delta P_c\right) \tag{7}$$

$$\Delta\dot{P}_c = K_s\beta\Delta f \tag{8}$$

with ΔP_m as the total power generated by Diesel Engines (DE), Thermal Turbines (TT), and Hydro Turbines (HT), thus P_g and T_g are the power output and time response of the governor of DE, TT, and HT. T_T and R_D are time responses and speed droop governors of DE, TT, and HT. ΔP_c represents Area Control Error (ACE) output. K_s is the constant of ACE, and β is the bias factor.

Besides that, the dynamic models of the electrical parts of the generators incorporating the AVR control loop and PSS are given in Equation (9) until Equation (11) [21], [22].

$$\Delta\dot{P}_e = \frac{1}{2H}\left(-K_1\Delta\delta - D\Delta\omega - K_2E_q\right) \tag{9}$$

$$\Delta\dot{E}_q = \frac{1}{T_{exc}}\left(K_4\Delta\delta - \frac{\Delta E_q}{K_3} + E_{fd}\right) \tag{10}$$

$$\Delta\dot{E}_{fa} = \frac{k_a}{T_a}\left(K_5\Delta\delta - K_6\Delta E_q - \Delta V_{PSS}E_{fd}\right) - \frac{E_{fa}}{T_a} \tag{11}$$

with K_1 is the synchronization coefficient between P_e and $\Delta\omega_R$ at constant flux. K_2 is the relation between P_e and flux in constant ω_R. E_q and E_{fd} are the terminal and the exciter output voltages, respectively. T_{exc}, K_3, and $K_4$are the time response, impedance factors, and demagnetization effect of the exciter, respectively. k_a and $T_a$are the gain constant and time response of the amplifier in the exciter. K_5 is the relationship between the voltage terminal change and $\Delta\delta$ in the constant E_q. K_6relates the terminal voltage change and E_q in the constant $\Delta\delta$. ΔV_{PSS} is the stability reference signal from PSS that is given by Equation (12) [21], [22].

$$\Delta V_{PSS} = K_{PSS}\left[\frac{sT_{wo}}{1+sT_{wo}}\right] \left[\frac{(1+T_1s)}{(1+T_2s)}\frac{(1+T_3s)}{(1+T_4s)}\right][\Delta f, \Delta\delta] \tag{12}$$

with K_{PSS} and $T_{wo}$are the gain and wash-out filters of the PSS. The tuneable parameters of the PSS are T_1, T_2, T_3, and T_4.

The PSS uses the Δf and $\Delta\delta$ as power system stability references, which can be obtained from the local or interarea responses. PSS provides ΔV_{PSS} to be fed to the AVR control loop by adjusting the tuneable parameters that determine the leading or lagging state of the system. The ΔV_{PSS} triggers the excitation system to increase or decrease the magnetic flux, producing ΔP_e with electrical torque (ΔT_e). The ΔT_e counteracts the mechanical torque (ΔT_m) to dampen the oscillation due to the disturbances.

The modified PSS2B-IEEE from [46] is used as in Fig. 2, which accommodates the dual input requirements. In addition, the typical tuning rules of this PSS model are described in Table 1. PSS2B-IEEE has three gain

TABLE 1. Typical tuning rules for PSS2B-IEEE in the proposed power systems.

Parameter	Value
K_{PSS1}	Tuneable [0.01, 10]
K_{PSS2}	$\frac{T_7}{2H}$
K_{PSS3}	1
T_{wo1}, T_{wo2}, T_{wo3}	10
T_{wo4}	Bypassed
T_1, T_2, T_3, T_4	Tuneable [0.01, 2]
T_6	Bypassed
T_7	T_{wo2}
T_8	0.3
T_9	0.15
M	2
N	4

constants: K_{PSS1}, K_{PSS2}, and K_{PSS3}; four wash-out filters: $T_{wo1}, T_{wo2}, T_{wo3}$, and$T_{wo4}$; eight lead or lag controllers: $T_1, T_2, T_3, T_4, T_6, T_7, T_8$, and T_9; ramp tracking features: M and N. In this paper, PSS2B-IEEE has five typical parameters to be tuned by HHO-MSS: K_{PSS1}, T_1, T_2, T_3, and T_4.

B. PROPOSED VIRTUAL INERTIA MODEL

In recent literature [23], [24], [25], the RES in VIC schemes are typically designed to inject power directly into the generator, limiting further investigation of the RES effects. This paper proposes a VIC design in which RES is connected to separated inverters, allowing the power output to be injected into the power system in two distinct modes. In the first mode, RES is directly injected into the system; meanwhile, in the second mode, RES power is directed into an ESS providing the reserve power. This reserve power, used for virtual inertia emulation, is regulated by VIC before being injected into the power system. For instance, this paper sets the RES power output to be injected with a 60% to 40% ratio between ESS and direct power to the system. The proposed model enables a deeper investigation of RES impact and adds flexibility to virtual inertia emulation. The dynamic model for the proposed VIC is given in Equation (13) and illustrated in Fig. 3.

$$\Delta P'_{VI} = \frac{1}{R_{VI} T_{ESS} T_{INV1}} \left(D_{VI} \Delta f + K_{VI} \dot{\Delta f}\right) + \Delta P_{WG} + \Delta P_{PV} - \frac{\Delta P_{VI}}{T_{INV1}} \tag{13}$$

with ΔP_{WG} and ΔP_{PV} are WG and PV power output that the dynamic models are given by Equation (14) and Equation (15), respectively. This paper is focused on the effect of RES level, so the uncertain and fluctuating behaviors are not taken into account. In this dynamic model, the WG and PV power outputs are assumed linearly affected by changes in wind speed and solar irradiance levels.

$$\Delta P_{WG} = \frac{1}{T_{WG} T_{INV2}} \left[\Delta V_W - \Delta P_{WG}\right] \tag{14}$$

$$\Delta P_{PV} = \frac{1}{T_{PV} T_{INV3}} \left[\Delta \Phi - \Delta P_{PV}\right] \tag{15}$$

with K_{VI} and D_{VI} are virtual inertia and virtual damping as tuneable parameters in VIC with values ranging from 0.01 to 2. The T_{INV1} and T_{ESS} are time responses of the VIC inverter and ESS, respectively. The R_{VI} is the droop constant of VIC. The ΔP_{WG} is affected by the wind speed change (ΔV_W), with T_{INV2} and T_{WG} are time responses of the WG inverter and WG, respectively. The ΔP_{PV} is affected by the solar irradiance change ($\Delta\Phi$), with T_{INV3} and T_{PV} are time responses of the PV inverter and PV, respectively.

C. STATE-SPACE MODEL FOR THE PROPOSED POWER SYSTEMS WITH PSS-VIC

The interconnected power system is transformed into the state-space model for ease of coding implementation. With the state-space model, coding and simulation can be performed more efficiently than using simulation blocks. The state-space model is represented by Equation (16).

$$\begin{aligned} \dot{x} &= Ax + Bu \\ y &= Cx \end{aligned} \tag{16}$$

with x is the matrix of observable system variables, u is the matrix of small-signal disturbance variables, y is output, A is the matrix of the system dynamic response, and B is the matrix of input. The x and u matrices are given by Equation (17) and Equation (22).

$$x^T = [x_1 x_2] \tag{17}$$

$$x_1 = \left[\Delta\delta_1 \Delta f_1 \Delta P_{m1} \Delta P_{g1} \Delta P_{c1} \Delta P_{e1} \Delta E_{q1} \Delta E_{fd1} \Delta P_{VI1} \Delta P_{WG1} \Delta P_{PV1}\right] \tag{18}$$

$$x_2 = \left[\Delta\delta_2 \Delta f_2 \Delta P_{m2} \Delta P_{g2} \Delta P_{c2} \Delta P_{e2} \Delta E_{q2} \Delta E_{fd2} \Delta P_{VI2} \Delta P_{WG2} \Delta P_{PV2}\right] \tag{19}$$

$$u^T = [u_1 u_2] \tag{20}$$

$$u_1 = [\Delta P_{L1} \Delta P_{m1} \Delta V_{PSS1} \Delta D_{VI1} \Delta K_{VI1} \Delta V_{W1} \Delta \Phi_1] \tag{21}$$

$$u_2 = [\Delta P_{L2} \Delta P_{m2} \Delta V_{PSS2} \Delta D_{VI2} \Delta K_{VI2} \Delta V_{W2} \Delta \Phi_2] \tag{22}$$

The completed state-space model for the interconnected power systems interfaced with PSS-VIC is given in Appendix.

III. PROPOSED PSS-VIC OPTIMIZATION

This section presents the problem formulation for optimizing the PSS-VIC design using HHO-MSS. The objective function, optimization variables, search space, and constraints are explained. The HHO-MSS implementation for PSS-VIC is described. An overview of EMA, EEFO, and PO is also presented.

A. FORMULATION FOR PSS-VIC OPTIMIZATION

This paper uses eigenvalue analysis to indicate the power system stability performance from the dynamic responses of

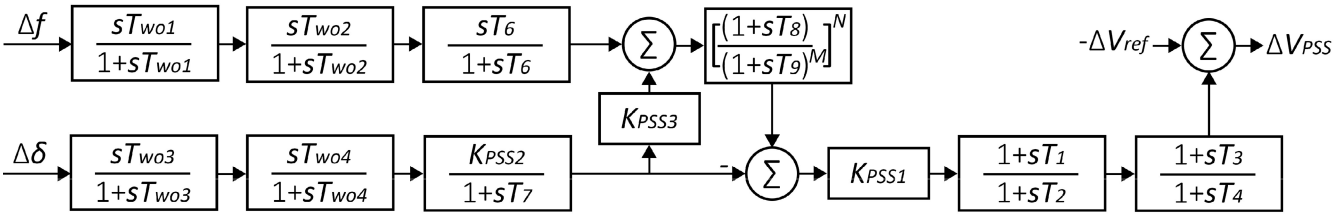

FIGURE 2. PSS2B-IEEE design in the proposed power systems.

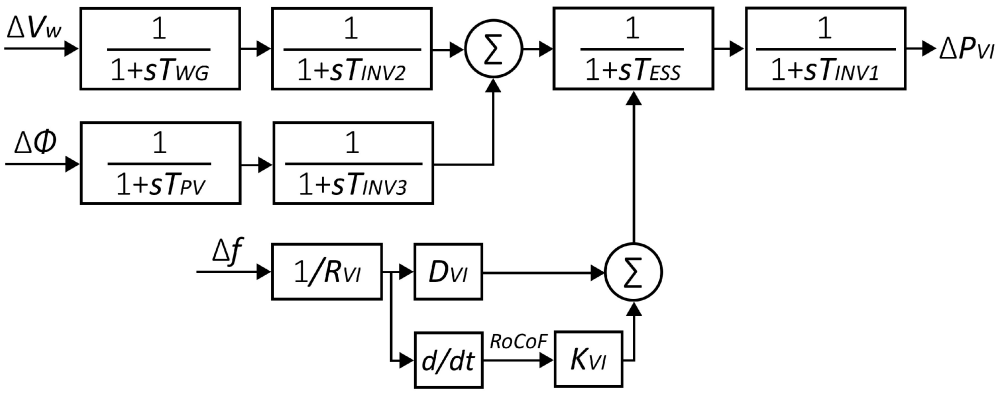

FIGURE 3. Proposed VIC design with RES integration in the proposed power systems.

TABLE 2. Search space for the tuneable parameter (TP) of PSS-VIC design optimization.

Tuneable Parameter	*lb*	*ub*
K_{PSSI}	0.01	10
T_1, T_2, T_3, T_4	0.01	2
K_{VI}	0.1	2
D_{VI}	0.1	10

the power systems. The eigenvalue of this system (λ) can be obtained by extracting the determinant of Equation (16) by using Equation (23) as Equation (24).

$$\det(\lambda I - A) = 0 \tag{23}$$

$$\lambda_A = \sigma_A \pm \omega_A i \tag{24}$$

with I is the identity matrix of the same order (n x n dimension) as matrix A. The $\lambda_A$consists of real (σ_A) and imaginary (ω_A) components, which represent the damping properties and frequency oscillations of the system, respectively. From the eigenvalue, the damping ratio of the system can be obtained as Equation (25).

$$\zeta_A = \frac{-\sigma_A}{\sqrt{\sigma_A^2 \pm \omega_A^2}} \tag{25}$$

The PSS-VIC optimization problem is formulated with the objective function that indicates a minimum damping ratio ($\zeta_{A,min}$), which represents the minimum level of damping value required to dampen the oscillation. The value of $\zeta_{A,min}$ should be maximized by controlling the tuneable parameters of the PSS-VIC as given by Equation (26). Because the fitness value in Equation (26) is reversed into $(1-f_{(x)})$, so it becomes a minimization function.

$$\min\left[\zeta_{A,i}\left(TP_j\right)\right] = \sum_{t_{sim}=1}^{t_{sim,max}} \left[1 - \zeta_{A,i}\left(TP_j\right)\right] \tag{26}$$

with TP is a set of parameters consisting of K_{PSS1}, $T_1, T_2, T_3, T_4, K_{VI}$, and D_{VI}, generated by algorithm. The i is the number of interconnected power system areas, while the j is the number of controllers.

The search space consisting of the lower bound (*lb*) and the upper bound (*ub*) of tuneable parameters is shown in Table 2. In most of the literature, the search process is not specifically constrained, so it takes a long time, and it is longer to reach the convergent result. So, this paper uses the D-shape region of power system stability shown in Fig. 4 as a constraint for coordinating PSS-VIC to significantly reduce the number of inappropriate candidate solutions [21], [22]. In this case, the real part of the eigenvalue in the next iteration ($\sigma_{A,1}$) should be more negative than in the previous iteration ($\sigma_{A,0}$). Meanwhile, the damping ratio in the next iteration ($\zeta_{A,1}$) should be better than the damping ratio in the previous iteration ($\zeta_{A,0}$). The better solution is indicated by the eigenvalue point shifted to the D-shape region. In addition, the optimization adheres to grid codes, which permit a damping ratio ranging from 5% to 10%, as higher damping ratios can result in unnecessarily

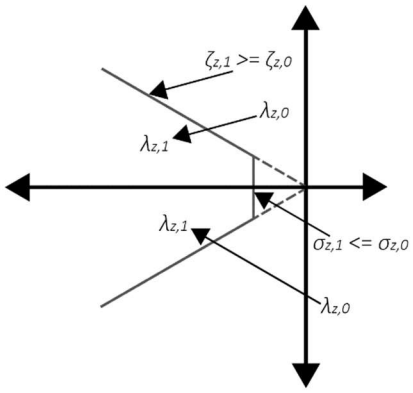

FIGURE 4. D-shape region of power system stability as a constraint for PSS-VIC design optimization.

slower responses. This paper uses grid code in Indonesia as the optimization reference [47].

In the literature, the performance indices are typically used as a final result validation, so it does not affect the quality of optimization [7], [8]. To increase the accuracy and ensure the quality of candidate solutions, the proposed procedure uses performance indices as constraints for the PSS-VIC design optimization, including Integral Time Absolute Error (ITAE), Integral Absolute Error (IAE), Integral Time Squared Error (ITSE), and Integral Squared Error (ISE), as shown in Equation (27) until Equation (30).

$$\text{ITAE} = \int_{t_{\text{sim}}=1}^{t_{s\ \text{simmax}}} t|e(t)|dt \tag{27}$$

$$IAE = \int_{t_{\text{sim}}=1}^{t_{\text{simmax}}} |e(t)|dt \tag{28}$$

$$\text{ITSE} = \int_{t_{sim}=1}^{t_{simmax}} te^2(t)dt \tag{29}$$

$$ISE = \int_{t_{\text{sim}}=1}^{t_{s\ \text{sinm max}}} e^2(t)dt \tag{30}$$

B. OPTIMIZING PSS-VIC DESIGN USING HHO-MSS

This section describes the implementation of HHO-MSS for optimizing PSS-VIC design which is divided into pre-hunting, exploration, transition, exploitation, and memory saving strategy phases.

1) PRE-HUNTING

In the first step, HHO-MSS generates a set of candidate solutions consisting of TP in Table 2 by Equation (31).

$$H_p = \left(lb \le H_p \le ub\right)^{Dim} \tag{31}$$

with $H_p$is the vector of the hawk based on the number of population ($p = 30$), and Dim is the dimension representing the number of tuneable parameters of PSS-VIC ($Dim = 14$).

The vector of the rabbit representing the best solution candidate is also generated as R with the initial energy of the rabbit (E_o). The value of E_o is a random value between -1 and 1. This value is used to calculate the remaining escaping energy of the rabbit as Equation (32).

$$E_{ESC} = 2E_o\left(1 - \frac{I_t}{I_{t,\max}}\right) \tag{32}$$

The hawks and rabbits dynamically move along the iterations (I_t) until the maximum iteration ($I_{t,max}$) is reached or the rabbit is caught by the hawks. However, the movements of the hawks are constrained by Equation (33) until Equation (35). These constraints reduce the unfavorable moves by the hawks.

$$H_{\sigma_{I_t+1}} \le H_{\sigma_{I_t}} \tag{33}$$

$$H_{\zeta_{I_t+1}} \ge H_{\zeta_{I_t}} \tag{34}$$

$$H_{PR_{I_t+1}} \le H_{PR_{I_t}} \tag{35}$$

Equation (33) and Equation (34) eliminate the candidate solution that does not satisfy the D-shape region of power system stability in Fig. 4. The damping properties of the candidate solution in the next iteration ($H_{\sigma_{I_t+1}}$) should be more negative than in the current iteration ($H_{\sigma_{I_t}}$). Moreover, the damping ratio of the candidate solution in the next iteration ($H_{\zeta_{I_t+1}}$) should be higher than in the current iteration ($H_{\zeta_{I_t}}$). While Equation (35) ensures that the value of ITAE, IAE, ITSE, and ISE of the candidate solution in the next iteration ($H_{PR_{I_t+1}}$) is lower than in the current iteration ($H_{PR_{I_t}}$).

2) EXPLORATION

The hawks do not chase the rabbit directly, however they observe and surround the rabbit by perching and moving from branches to other branches approaching the rabbit. The hawks wait for the rabbit to let the guard down before they start hunting. The movement is determined by q. If $q \ge 0.5$, then the hawks move randomly as in Equation (36), while q <0.5, then the hawks approach the rabbit as in Equation (37).

$$H\left(I_t + 1\right) = H_r\left(I_t\right) - r_1\left|H_r\left(I_t\right) - 2r_2H\left(I_t\right)\right| \tag{36}$$

$$H\left(I_t + 1\right) = \left[R\left(I_t\right) - H_{\text{avg}}\left(I_t\right)\right] - r_3\left[ub + r_4(ub - lb)\right] \tag{37}$$

with H_r is a random hawk and H_{avg} is the average distance between the hawks and the rabbit as given in Equation (38). The r_1, r_2, r_3, and r_4 are randomly distributed values between o to 1.

$$H_{\text{avg}}\left(I_t\right) = \frac{1}{p}\sum_{p}^{p,\max} H\left(I_t\right) \tag{38}$$

3) TRANSITION

If $E_o = 0 \rightarrow 1$, it indicates the rabbit is still alert to the situation, while $E_o = 0 \rightarrow -1$, then the rabbit seems careless with the situation, thus hawks will begin hunting. The transition is determined by $|E_{ESC}|$ as follows: 1) If $|E_{ESC}| \ge 1$, then the hawks continue the exploration; 2) If $|E_{ESC}| < 1$, then the hawks begin the exploitation.

4) EXPLOITATION

The exploitation mechanism is divided into four schemes dependent on rabbit conditions represented by $|E_{ESC}|$ and escape probability (r_{ESC}). r_{ESC} is a random value between 0 and 1. If $r_{ESC} \geq 0.5$, then the escape probability is higher, while$r_{ESC}< 0.5$, then the escape probability is lower.

Soft besiege is executed when $|E_{ESC}| \geq 0.5$ and $r_{ESC} \geq 0.5$, representing the hawks surrounding the rabbit are confused and tired. The equation is given in Equation (39).

$$|H\,(I_t+1) = \Delta H\,(I_t) - E_{ESC}||_R\,R\,(I_t) - H\,(I_t)\,| \quad (39)$$

with $\Delta H\,(I_t) = R\,(I_t) - H\,(I_t)$, $J_R$is the jumping movement of the rabbit as $2(1 - r_5)$, and r_5 is a randomly distributed value between 0 to 1.

Hard besiege is executed when $|E_{ESC}| < 0.5$ and $r_{ESC} \geq 0.5$, representing the rabbit that begins to be tired, thus the hawks shock the rabbit with hard besiege. The equation is given in Equation (40).

$$H\,(I_t+1) = R\,(I_t) - E_{ESC}\,|\Delta H\,(I_t)| \quad (40)$$

Soft besiege with rapid dives is executed when $|E_{ESC}| \geq 0.5$ and $r_{ESC} < 0.5$, representing the rabbit's success in escaping with Levy Flight (LF) moves as in [48]. Thus, the hawks perform rapid dives predicting the rabbit moves (R_Y) based on LF as Equation (41). If failed, the hawks re-predict the rabbit moves again (R_W) based on Equation (42).

$$|H\,(I_t+1) = R_Y = R\,(I_t) - E_{ESC}|\,J_R R\,(I_t) - H\,(I_t)\,| \quad (41)$$

$$H\,(I_t+1) = R_W = R_Y + S \times LF(\mathrm{Dim}) \quad (42)$$

with S is a random matrix 1 x Dim.

Hard besiege with rapid dives is executed when $|E_{ESC}| < 0.5$ and $r_{ESC} < 0.5$, representing the rabbit is tired due to continuous besieges from the hawks. Thus the hawks perform rapid dives until the rabbit is caught. The equation for $R_Y$is changed into Equation (43), while $R_W$is the same with Equation (42).

$$|\,H\,(I_t+1) = R_Y = R\,(I_t) - E_{ESC}\,V_R R\,(I_t) - H_{\mathrm{avg}}\,(I_t)\,| \quad (43)$$

The hunting process is terminated when the rabbit is caught by the hawks, as indicated with $|E_{ESC}| \to 0$ and the fitness value of the hawks is smaller than E_{ESC}, or the maximum iteration is reached.

5) MEMORY SAVING STRATEGY

Based on [21], the MSS is adopted from the operator of the Equilibrium Optimizer (EO) to improve the balance of exploration and exploitation processes in HHO. The idea is to sort the best hawk movements (H_{pool}) by Equation (44).

$$H_{pool} = \left[\left(H_1, H_2, H_3, \ldots, H_p\right)\right] \quad (44)$$

The component of H_{pool} is updated regularly along the iterations based on Equation (45) to adjust the hawks's next moves. If the current move of the hawks is better than the next move, the current move should be kept. While the next move by the hawks is better than the previous move, the move is changed to the other direction.

$$H_{\mathrm{pool}} = \begin{cases} H\,(I_t+1) < H\,(I_t)\,, & H_p = H\,(I_t) \\ H\,(I_t+1) > H\,(I_t)\,, & H_p = H\,(I_t+1) \end{cases} \quad (45)$$

C. COMPARISON ALGORITHMS

This paper uses EMA, EEFO, and PO as proposed to be compared with HHO-MSS performance. EMA is one of the novel bio-inspired metaheuristic algorithms introduced to solve the constrained optimization cases by Sulaiman, et al. in 2023 [43]. This algorithm simulates the randomness of the mating processes of the organism. The main optimization concept of this algorithm is formulated based on the equilibrium and crossover indices by Hardy–Weinberg in the offspring production.

EEFO is a novel swarm-based and bio-inspired metaheuristic algorithm developed by Zhao, et al. in 2024 [44]. This algorithm is formulated to be a parameter-free optimizer, thus it is easy to implement. EEFO adopted the intelligent foraging group of electric eels. In nature, electric charge produced by electric eels is considered one of the highly advanced features in animals, especially for communication purposes. The unique exploration and exploitation mechanism is formulated by simulating the foraging processes, including interaction, resting, hunting, and migration of the electric eels.

PO is a recent novel bio-inspired metaheuristic algorithm proposed by Abdollahzadeh, et al. in 2024 [45]. Puma is considered one of the animals with very good intelligence and memory features. Puma can drag their potential prey to specific places, cover it with bushes, and hunt it with the group in the next several days. This algorithm simulates the transition behavior of inexperienced puma into experienced ones in exploring and exploiting their prey.

IV. SIMULATION AND DISCUSSION

The simulation is conducted in MATLAB 2022b environment with the following equipment specifications: Processor AMD Ryzen 5 5600H (12 CPU) with 3.3 GHz; SSD Micron 512 GB NVMe M.2; RAM DDR4 16 GB with dual-channel configuration; and NVIDIA GeForce GTX 1650 4 GB. The power system is simulated with detailed parameters as shown in Table 3, and the parameters for algorithms are presented in Table 4. Various simulations are performed to investigate the scalability of the PSS-VIC design in improving the power system stability, as given in the following.

1) **Simulation 1: Load Variation**
   This simulation examines the capability of the PSS-VIC design to improve power system stability

TABLE 3. Simulation parameters for the proposed power systems.

Parameter	Value	
	Area 1	Area 2
H, total inertia of the base system	9.6	6.8
D, damping value of the base system	0.82	0.57
T_{DE}, time response of DE	0.54	0.25
T_{TT}, time response of TT	0.52	0.24
T_{HT}, time response of HT	0.48	0.19
T_{g1}, time response of DE	0.27	0.13
T_{g2}, time response of TT	0.25	0.11
T_{g3}, time response of HT	0.23	0.09
R_D, droop constant	19.7	18.4
β, bias factor	20.15	18.9
T_a, time response of the amplifier	0.06	0.04
k_a, gain constant of the amplifier	50	50
T_{exc}, time response of the exciter	5.8	4.9
K_1, synchronization coefficient	1.33	1.32
K_2, constant of P_e and flux	0.94	0.93
K_3, impedance factor of the exciter	0.43	0.41
K_4, demagnetization effect of the exciter	1.7	1.68
K_5, constant of terminal voltage and $\Delta\delta$	0.06	0.04
K_6, constant of terminal voltage and E_q	0.67	0.64
T_{WG}, time response of WG	1.4	1.3
T_{PV}, time response of PV	1.9	1.8
T_{ESS}, time response of ESS	0.05	0.04
T_{INV1}, time response of PV inverter	0.01	0.01
T_{INV2}, time response of WG inverter	0.02	0.02
T_{INV3}, time response of PV inverter	0.03	0.03
R_{VI}, droop constant of VIC	2	2

after sudden load changes consisting of load addition and load shedding.

2) **Simulation 2: Inertia Variation**
This simulation measures the effectiveness of the PSS-VIC design when implemented in power systems characterized by low inertia or high inertia.

3) **Simulation 3: RES Level Variation**
This simulation is conducted to investigate the adaptability of the PSS-VIC design to improve power system stability in low and high RES levels.

The discussion is divided into two sections, the first section focuses on the performance comparison of algorithms in finding the optimal design of PSS-VIC, and the second one focuses on the detailed explanation of the PSS-VIC design examination in various proposed simulations and the result discussion regarding the power stability improvement.

A. PERFORMANCE COMPARISON OF ALGORITHM IN CONDUCTING OPTIMAL DESIGN OF PSS-VIC

In this section, the statistical assessment and convergence curve analysis are conducted to validate the algorithm performance in performing the optimal design of PSS-VIC. The statistical assessments of the algorithms in finding the optimal design of PSS-VIC are tabulated in Table 5. The assessment is conducted based on 30 runs and 100 iterations with 30 search agents of the algorithms in three kinds of simulations for calculating the equilibrium point of the global

TABLE 4. Simulation parameters for the algorithms.

Parameter	Algorithm			
	HHO-MSS	EMA	EEFO	PO
Run	30	30	30	30
$I_{t,max}$	100	100	100	100
N_{pop}	30	30	30	30
Dim	14	14	14	14
q	rand [0, 1]	-	-	-
r_1, r_2, r_3, r_4,	rand [0, 1]	-	-	-
p	-	rand [0, 1]	-	-
q	-	$1-p$	-	-
C_r	-	0.8	-	-
r	-	0.2	-	-
PF1	-	-	-	0.5
PF2	-	-	-	0.5
PF3	-	-	-	0.3
U	-	-	-	0.2
L	-	-	-	0.8
α	-	-	-	1

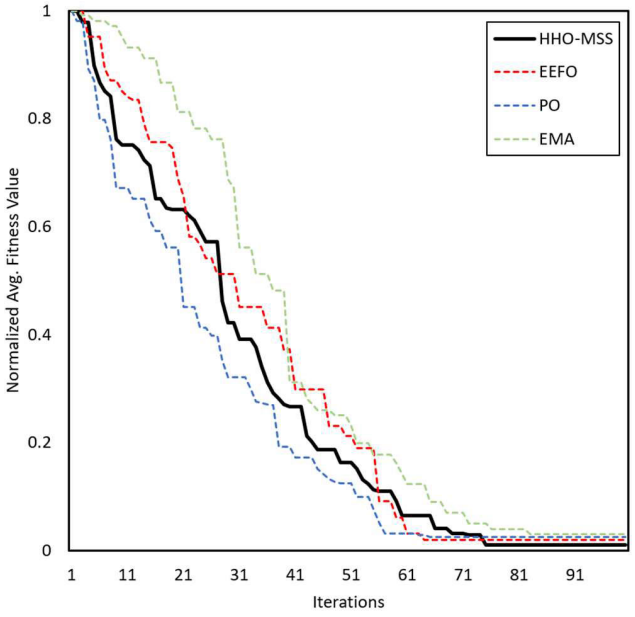

FIGURE 5. Convergence curve of normalized average fitness value of HHO-MSS, EEFO, PO, and EMA.

parameters of PSS-VIC. The tabulated fitness values are normalized from 0 to 1 to provide a fair comparison. In this normalization, the fitness value closer to 0 means a better solution.

The average and standard deviation (std. dev.) values present the accuracy and consistency of the algorithms, respectively. Based on Table 5, HHO-MSS has the best ranking based on the average and standard deviation values, followed by EEFO, PO, and EMA. The overall average value of HHO-MSS is 1.05×10^{-1}, which is 1.44%, 3.45%, and 9.28% better than EEFO, PO, and EMA, respectively. Moreover, the overall standard deviation value by HHO-MSS of 7.8×10^{-3}, which is 34.63%, 48.05%, and 53.94% better

TABLE 5. Statistical result of the optimal solution by HHO-MSS, EEFO, PO, and EMA.

Simulation	Statistics	Algorithm			
		HHO-MSS	EEFO	PO	EMA
1	Average	1.07×10^{-1}	1.06×10^{-1}	1.1×10^{-1}	1.07×10^{-1}
	Std. Dev.	1.82×10^{-3}	4.34×10^{-3}	5.16×10^{-3}	5.61×10^{-3}
2	Average	6.95×10^{-2}	7.06×10^{-2}	7.13×10^{-2}	8.29×10^{-2}
	Std. Dev.	3.19×10^{-3}	4.56×10^{-3}	7.51×10^{-3}	9.41×10^{-3}
3	Average	1.09×10^{-1}	1.13×10^{-1}	1.15×10^{-1}	1.24×10^{-1}
	Std. Dev.	5.77×10^{-3}	7.6×10^{-3}	8.09×10^{-3}	8.41×10^{-3}
Overall Average		1.05×10^{-1}	9.51×10^{-2}	9.65×10^{-2}	9.85×10^{-2}
Overall Std. Dev.		7.8×10^{-3}	3.59×10^{-3}	5.5×10^{-3}	6.92×10^{-3}
Rank		1	2	3	4

TABLE 6. Global parameters of PSS-VIC conducted by HHO-MSS, EEFO, PO, and EMA.

Algorithm	Parameter													
	$K_{PSS1,1}$	$T_{1,1}$	$T_{2,1}$	$T_{3,1}$	$T_{4,1}$	$K_{VI,1}$	$D_{VI,1}$	$K_{PSS1,2}$	$T_{1,2}$	$T_{2,2}$	$T_{3,2}$	$T_{4,2}$	$K_{VI,2}$	$D_{VI,2}$
HHO-MSS	5.685	1.527	0.582	1.599	1.102	0.852	6.459	5.374	1.088	1.068	1.574	0.961	0.873	1.404
EEFO	6.243	1.477	0.567	0.665	0.404	0.341	5.159	4.106	0.384	0.688	0.43	1.168	1.691	2.625
PO	4.416	1.208	1.025	1.02	0.636	0.881	3.734	2.193	0.728	0.36	0.998	1.1	0.831	2.521
EMA	2.980	0.401	0.907	0.549	1.092	1.025	4.025	4.935	0.924	0.45	0.254	0.694	0.991	2.413

than EEFO, PO, and EMA, respectively. This result concludes that HHO-MSS has the best accuracy and consistency over the EEFO, PO, and EMA in finding the global parameters of PSS-VIC. The accuracy and consistency of the algorithms ensure the optimal PSS-VIC design is accurate and not biased.

Besides that, the historical process of the algorithms in conducting their best solution is illustrated in the normalized average fitness values curve as in Fig. 5. In the short-iteration run like in the first 50 iterations, PO has the best characteristics, followed by HHO-MSS, EEFO, and EMA. However, in the long-iteration run, the convergence curve can be different. It can be seen in the second 50 iterations of Fig. 5, the best solution of PO is overlapped by HHO-MSS and EEFO. Thus, in the final 100 iterations, HHO-MSS achieves the best solution, followed by EEFO, PO, and EMA. This result shows that the HHO is still a viable option among the algorithms that are four to five years newer.

B. PERFORMANCE INVESTIGATION OF PSS-VIC DESIGN IN IMPROVING POWER SYSTEM STABILITY

The global parameters of PSS-VIC are tabulated based on the equilibrium point of PSS and VIC parameters obtained in various simulations that perform the best power system stability effect. First, Simulation 1 is performed by changing the load condition ranging from -0.5 p.u. to 0.5 p.u. with 0.05 steps. Thus, this simulation justifies the best PSS-VIC design for 10 steps of load shedding and 10 steps of load addition. Second, Simulation 2 is executed by reducing the total inertia of the system by 20% to 50% with 5% steps. Thus, this simulation averages the best PSS-VIC design for six different inertia levels, ranging from high to low. Third, Simulation 3 simulates the RES level condition of 20% to 80% with 5% steps. Thus, this simulation concludes the global parameters of PSS-VIC from 12 RES levels, ranging from low to high RES levels. From a total of 38 different simulations, the equilibrium point of the global parameters of PSS-VIC can be tabulated as the optimal coordinated PSS-VIC design.

The global parameters of PSS-VIC conducted by HHO-MSS, EEFO, PO, and EMA are tabulated in Table 6. The first validation of the global parameters of PSS-VIC is performed by observing the eigenvalue of the power system in the local area mode of Area 1, local area mode of Area 2, and interarea mode which are tabulated in Table 7, Table 8, and Table 9, respectively. Table 7 until Table 9 present the eigenvalue around the equilibrium point that can be used to justify the power system stability. Several stability criteria should be fulfilled in the stable power system, as follows: 1) the existence of real and imaginary parts of the eigenvalues; 2) all real parts of the eigenvalues have a negative number. Thus, the tabulated eigenvalues in Table 7 until Table 9 have fulfilled the first criteria. This result justifies the utilization of the D-shape region of stability as a constraint formulated in Equation (32) until Equation (33) for PSS-VIC optimization is properly worked.

Based on Table 7 until Table 9, all of the algorithms produce the negative values on the real part of eigenvalues in the local area mode in Area 1 and Area 2, and in the interarea mode of the system. Besides that, the imaginary part of the eigenvalues consists of positive and negative values which represent the potential oscillation that occurred in the system. In addition, all of the damping ratios obtained by algorithms comply with the grid codes. PSS-VIC by HHO-MSS offers the best damping ratio (ζ) in both local and interarea responses. In the local area response of Area 1, ζ obtained by

TABLE 7. Eigenvalues in the local area mode of the power system in Area 1.

HHO-MSS PSS-VIC	EEFO PSS-VIC	PO PSS-VIC	EMA PSS-VIC
-17.9017 ± 1.9366i	-8.1955 ± 5.0775i	-8.5424 ± 5.4856i	-8.5410 ± 5.4952i
-2.7576 ± 9.6549i	-0.5857 ± 3.2671i	-0.8741 ± 0.0624i	-0.1626 ± 0.0691i
-1.1252 ± 1.6540i	-0.1191 ± 0.1151i	-0.1358 ± 0.0985i	-0.0947 ± 2.9579i
-0.1347 ± 0.1156i		-0.1262 ± 3.0027i	
ζ = 9.94%	**ζ = 8.51%**	**ζ = 8.41%**	**ζ = 8.4%**

TABLE 8. Eigenvalues in the local area mode of the power system in Area 2.

HHO-MSS PSS-VIC	EEFO PSS-VIC	PO PSS-VIC	EMA PSS-VIC
-18.5331 ± 1.7818i	-12.0687 ± 3.2802i	-11.0625 ± 2.9131i	-12.7642 ± 3.6413i
-9.7298 ± 2.7101i	-1.2192 ± 5.5897i	-0.9214 ± 5.7323i	-0.8840 ± 5.2824i
-1.5647 ± 6.5821i	-0.1122 ± 0.1355i	-0.1156 ± 0.1346i	-0.1239 ± 0.1298i
-0.0987 ± 0.1401i			
ζ = 9.95%	**ζ = 9.94%**	**ζ = 9.67%**	**ζ = 9.61%**

TABLE 9. Eigenvalues in the interarea mode of the power system.

HHO-MSS PSS-VIC	EEFO PSS-VIC	PO PSS-VIC	EMA PSS-VIC
-18.4231 ± 1.6828i	-17.9017 ± 1.9366i	-15.7642 ± 3.6413i	-12.0597 ± 3.2730i
-9.7348 ± 2.7509i	-11.0625 ± 2.9131i	-8.5410 ± 5.4952i	-8.1955 ± 5.0775i
-8.5424 ± 5.4856i	-2.7576 ± 9.6549i	-0.8842 ± 5.2823i	-1.1793 ± 5.5995i
-1.5847 ± 6.5212i	-1.1250 ± 1.6540i	-0.1366 ± 0.2033i	-0.5852 ± 3.2673i
-0.8745 ± 0.0631i	-0.9214 ± 5.7322i	-0.0941 ± 2.9581i	-0.1109 ± 0.2029i
-0.1258 ± 3.0028i	-0.1165 ± 0.2097i		
ζ = 9.96%	**ζ = 9.94%**	**ζ = 9.74%**	**ζ = 9.65%**

HHO-MSS is 9.94%, which is followed by EEFO, PO, and EMA of 8.51%, 8.41%, and 8.4%, respectively. In the local area response of Area 2, ζ obtained by HHO-MSS is 9.95%, which is followed by EEFO, PO, and EMA of 9.94%, 9.67%, and 9.61%, respectively. In interarea response, ζ obtained by HHO-MSS is 9.96%, which is followed by EEFO, PO, and EMA of 9.94%, 9.74%, and 9.65%, respectively.

Based on the eigenvalue analysis, HHO-MSS produces the optimal design of PSS-VIC with the most appropriate damping ratio to be implemented in both local areas and interarea modes. In the next section, the discussion is focused on the validation of the scalability of PSS-VIC in improving power system stability which is investigated by time domain simulation. The detailed power system stability responses are also tabulated, including the performance index validation.

1) SIMULATION 1: LOAD VARIATION

In this simulation, the capability of the PSS-VIC design to mitigate the small-signal oscillation due to sudden load changes consisting of load addition and load shedding was examined. Fig. 6, Fig. 7, and Fig. 8 give the performance samples of PSS-VIC in Simulation 1 by observing the responses of Δf_1, Δf_2, $\Delta\delta_1$, $\Delta\delta_2$, ΔV_{t1}, and ΔV_{t2}.

Fig. 6 with $\Delta P_{LTOT} = +0.5$ p.u. (50% of the nominal capacity), simulates the large number of loads that are suddenly added. Fig. 7 shows the simulation of $\Delta P_{LTOT} = +0.01$ p.u. (1% of the nominal capacity) representing the very small load addition. Fig. 8 with $\Delta P_{LTOT} = -0.3$ p.u. (-30% of the nominal capacity) presents the load shedding is suddenly occurred. From this simulation, it can be seen that VIC gives a better stability effect than PSS. Then, the PSS-VIC design by HHO-MSS produces a significant improvement over VIC or PSS only, followed by EEFO and PO. Meanwhile, the PSS-VIC design by EMA is not significantly different from PSS or VIC only. It means that the metaheuristic algorithm choice is very important to be considered in optimizing the PSS-VIC design.

Besides that, the optimal coordinated design of PSS-VIC is also examined in dynamic load changes as shown in Fig. 9. In this simulation, the ΔP_{LTOT} occurred at 2 s, 5 s, and 7 s time simulations of $+0.01$ p.u., -0.03 p.u., and $+0.02$ p.u., respectively. Since the capacity in Area 1 is larger than in Area 2, oscillations of Δf_1 and $\Delta\delta_1$ are more difficult to dampen than those of Δf_2 and $\Delta\delta_2$. Thus, the PSS-VIC effect is seen better than PSS or VIC only, while the responses in Area 2 are similar. In both V_{t1} and V_{t2} responses, PSS-VIC is superior to PSS or VIC alone in suppressing the voltage surge. Although PSS-VIC focuses on frequency stability, it also has a stability effect on the voltage responses.

Further investigation is performed by observing the statistical performances of PSS-VIC design in dynamic load changes shown in Table 10. By observing Δf_{tie} and ΔP_{tie}, the overall power system stability performance can be justified. VIC gives a better stability effect than PSS, thus PSS is considered as a base case to calculate the improvement percentage. The optimal design of PSS-VIC by HHO-MSS

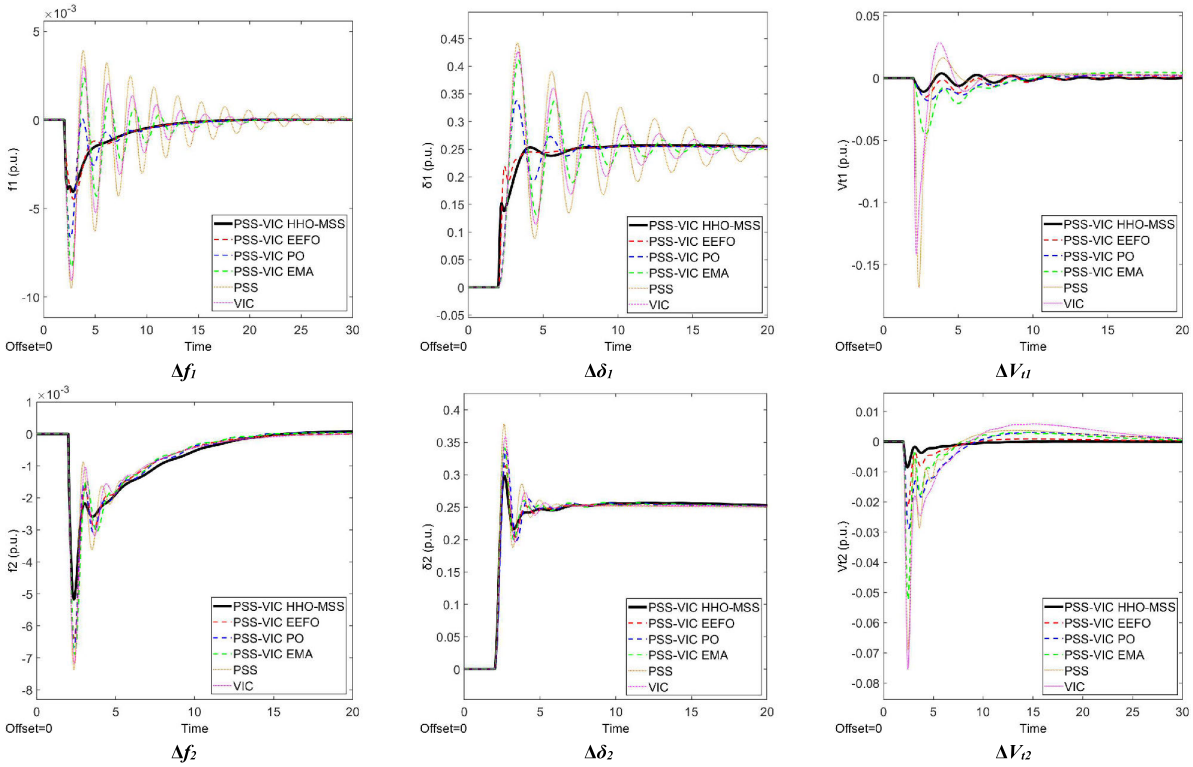

FIGURE 6. Performance of coordinated design of PSS-VIC in Simulation 1: $\Delta P_{LTOT} = +0.5$ p.u.

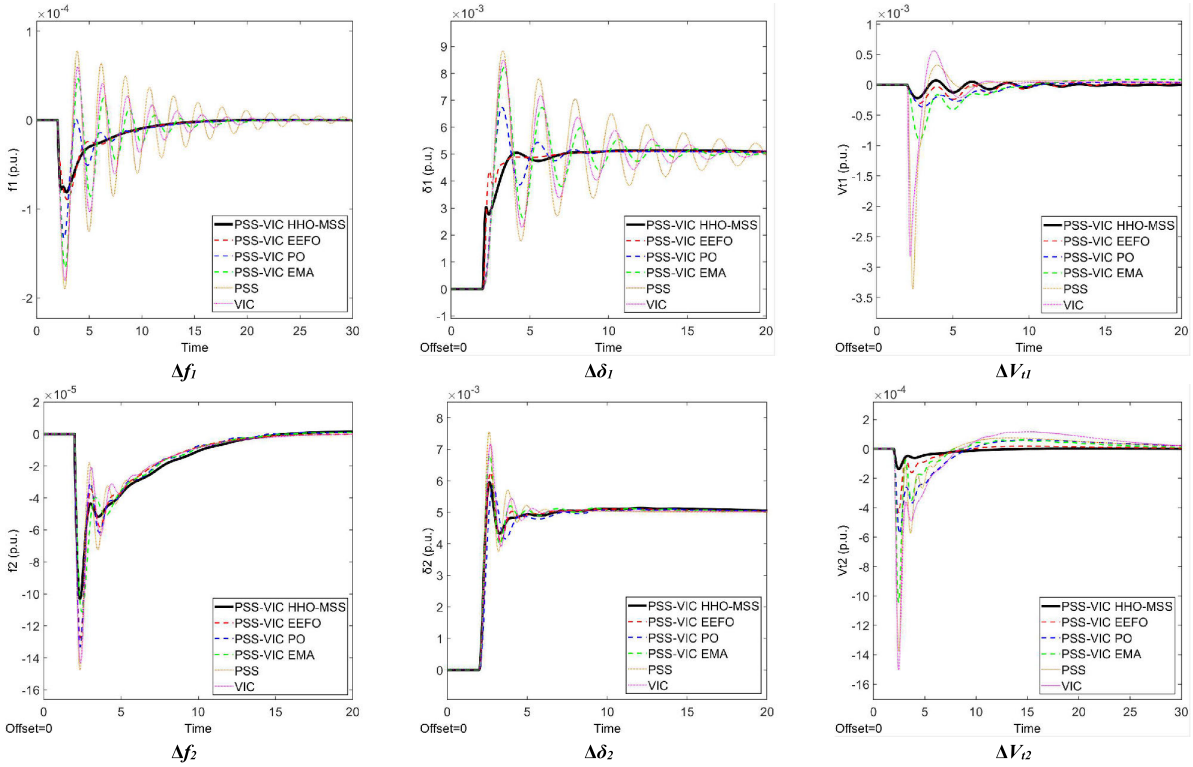

FIGURE 7. Performance of coordinated design of PSS-VIC in Simulation 1: $\Delta P_{LTOT} = +0.01$ p.u.

dampens the maximum deviation in Δf_{tie} of 2.07×10^{-4} p.u., which is 55.29% better than the base case. Moreover, PSS-VIC by HHO-MSS has also reduced the Δf_{tie} settling time of 2.77 s, which is 85.26% better than the base case

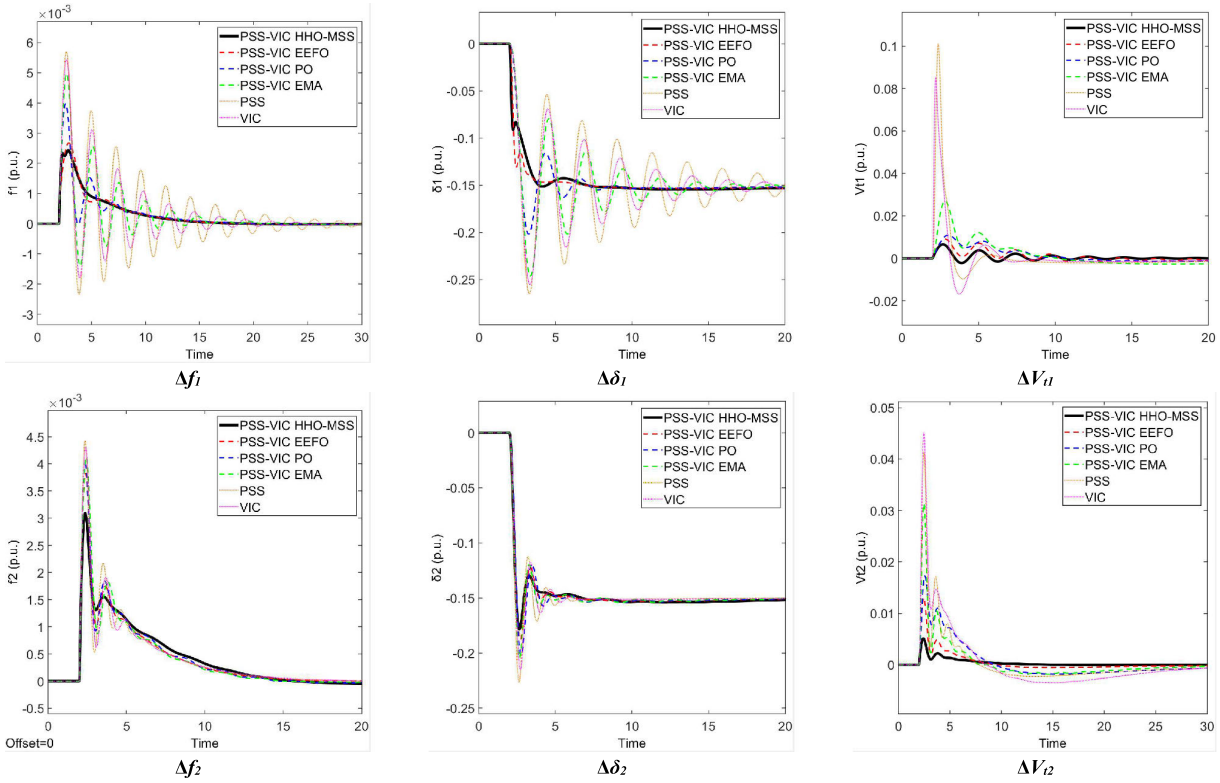

FIGURE 8. Performance of coordinated design of PSS-VIC in Simulation 1: $\Delta P_{LTOT} = -0.3$ p.u.

(settling time is measured when entering the steady-state response or equilibrium point after the last load changes in $t_{sim} = 7$ s occurred). The average error reduction of Δf_{tie} is calculated through performance indices of ITAE, IAE, ITSE, and ISE.

It is seen that PSS-VIC by HHO-MSS has the best average error reduction of 87.41% from the base case. The second-best result In Δf_{tie}, is PO, followed by EEFO and EMA.

Besides that, the stability of ΔP_{tie}response is very important to be investigated due to it represents the oscillation that occurs when the power is exchanged between areas through the tie line. The positive value means power exchanged from Area 1 into Area 2, while the negative value means power exchanged from Area 2 into Area 1. The largest oscillation occurred around $t_{sim} = 7$ s due to the accumulation of the previous oscillations that were not fully damped. PSS-VIC design by HHO-MSS produces the best improvement of maximum oscillation and settling time in $\Delta P_{tie}$by 67.38% and 84.83% of 1.52×10^{-4}p.u. and 2.78 s, respectively. PSS-VI by HHO-MSS produces the best average error reduction calculated by performance indices in $\Delta P_{tie}$of 89.08%. The second-best stability effect in ΔP_{tie} is offered by EEFO, followed by PO and EMA.

2) SIMULATION 2: INERTIA VARIATION

In this simulation, the effectiveness of PSS-VIC to be implemented in certain inertia levels is examined. In this section, the investigation is focused on high and low levels of inertia with 20% and 50% reduction of total inertia of the system, respectively. The analysis is more focused on the frequency nadir improvement related to RoCoF of the system when small disturbances occurred.

The small disturbances are simulated based on ΔP_L that occurred at $t_{sim} = 2$ s of +0.2 p.u. The power system adjusted the supplied power based on RES and conventional generators. The RES involvement makes the oscillation more complicated due to the different behavior of the RES. This paper considers that the RES capacity of Area 1 is greater than Area 2, however the time response of RES in Area 2 is faster than Area 1. Moreover, the size of WG is larger than PV, and the time response of PV is faster than WG. In this simulation, the RES penetration level is assumed to be 50% of the total generation. Thus, the generated power is assumed as follows: $\Delta P_{m1} = +0.05$ p.u., $\Delta P_{m2} = +0.05$ p.u., $\Delta V_{W1} = +0.03$ p.u., $\Delta V_{W2} = +0.03$ p.u., $\Delta \Phi_1 = +0.02$ p.u., and $\Delta \Phi_2 = +0.02$ p.u.

Time domain simulation results of Simulation 2 in high and low inertia levels are illustrated in Fig. 10 and Fig. 11, respectively. In addition, the frequency nadir comparison and the performance indices validation are presented in Table 11 and Table 12, respectively. The effectiveness of PSS and VIC can be deeply investigated with the proposed PSS-VIC design due to the effect of RES integration in virtual inertia emulation becomes clear.

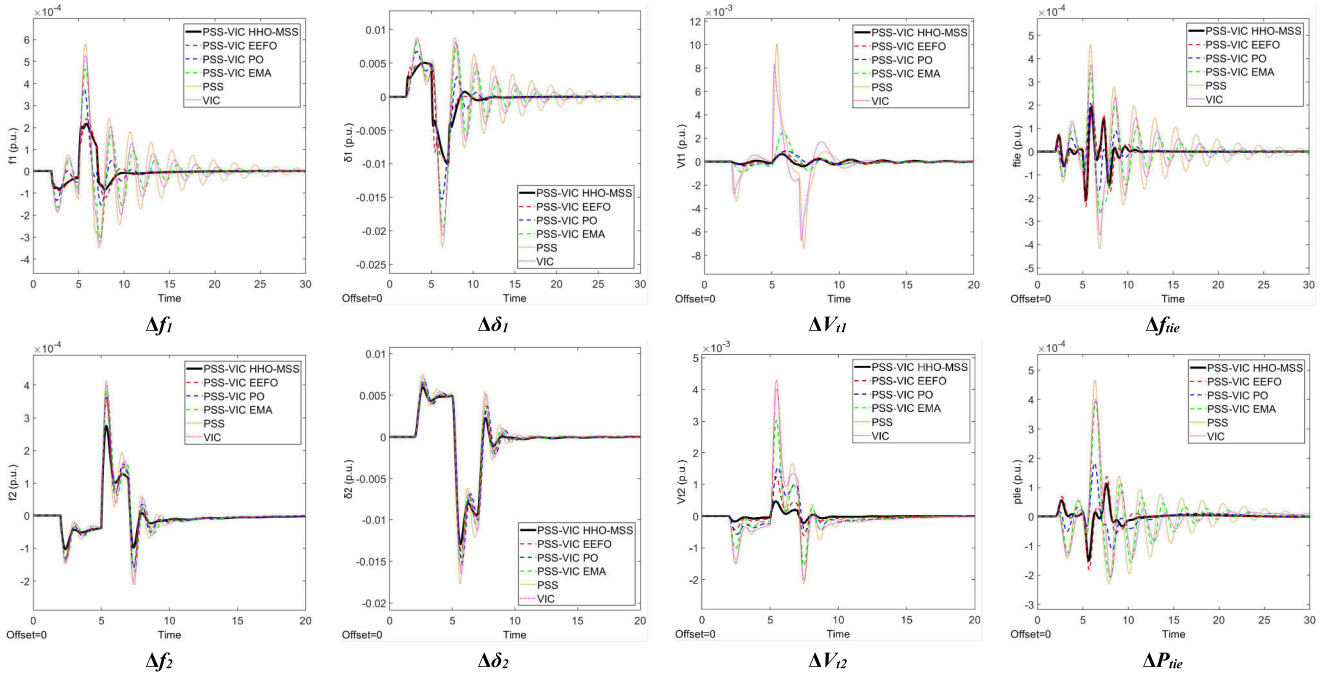

FIGURE 9. Performance of coordinated design of PSS-VIC in Simulation 1: Dynamic load changes.

TABLE 10. Statistical performance of coordinated design of PSS-VIC in Simulation 1: Dynamic load changes.

Response	Controller	Max. Deviation (p.u.)	Improve (%)	Settling Time (s)	Improve (%)	ITAE	IAE	ITSE	ISE	Avg. Error Reduction (-%)
Δf_{tie}	PSS	4.63 x 10^{-4}	-	18.79	-	2.23 x 10^{-2}	2.11 x 10^{-3}	3.09 x 10^{-6}	3.77 x 10^{-7}	-
	VIC	3.73 x 10^{-4}	19.65	13.35	28.95	1.42 x 10^{-2}	1.53 x 10^{-3}	1.84 x 10^{-6}	2.41 x 10^{-7}	35.08
	PSS-VIC HHO-MSS	2.07 x 10^{-4}	**55.29**	2.77	**85.26**	2.55 x 10^{-3}	4.03 x 10^{-4}	2.62 x 10^{-7}	4.27 x 10^{-8}	**87.41**
	PSS-VIC EEFO	2.35 x 10^{-4}	49.24	3.29	82.49	3.18 x 10^{-3}	4.94 x 10^{-4}	3.74 x 10^{-7}	5.95 x 10^{-8}	83.62
	PSS-VIC PO	2.09 x 10^{-4}	54.86	2.91	84.51	3.28 x 10^{-3}	4.81 x 10^{-4}	2.89 x 10^{-7}	4.55 x 10^{-8}	85.26
	PSS-VIC EMA	3.38 x 10^{-4}	27.01	9.27	50.67	1.07 x 10^{-2}	1.25 x 10^{-3}	1.34 x 10^{-6}	1.84 x 10^{-7}	50.15
ΔP_{tie}	PSS	4.66 x 10^{-4}	-	18.32	-	1.72 x 10^{-2}	1.65 x 10^{-3}	2.13 x 10^{-6}	2.7 x 10^{-7}	-
	VIC	4.01 x 10^{-4}	13.95	8.85	51.69	1.13 x 10^{-2}	1.21 x 10^{-3}	1.42 x 10^{-6}	1.99 x 10^{-7}	30.15
	PSS-VIC HHO-MSS	1.52 x 10^{-4}	**67.38**	2.78	**84.83**	2.33 x 10^{-3}	2.93 x 10^{-4}	1.17 x 10^{-7}	1.85 x 10^{-8}	**89.08**
	PSS-VIC EEFO	1.81 x 10^{-4}	61.16	2.94	83.95	2.99 x 10^{-3}	3.99 x 10^{-4}	2.1 x 10^{-7}	3.26 x 10^{-8}	84.12
	PSS-VIC PO	1.83 x 10^{-4}	60.73	4.02	78.06	4.57 x 10^{-3}	4.98 x 10^{-4}	2.46 x 10^{-7}	3.46 x 10^{-8}	79.72
	PSS-VIC EMA	3.93 x 10^{-4}	15.67	11.91	34.99	1.17 x 10^{-2}	1.24 x 10^{-3}	1.39 x 10^{-6}	1.86 x 10^{-7}	30.67

At high inertia level, the total inertia of the power system is reduced by 20% ($H_1 = 7.68$, $H_2 = 5.44$). In this simulation, the small disturbance is simulated as $\Delta P_L = +0.2$ p.u. (20% of the nominal capacity) which can significantly increase the frequency nadir of Δf_1, Δf_2, and Δf_{tie}. Fortunately, it can be seen clearly that the frequency nadir can be suppressed under 2% (0.02 p.u.) by PSS, VIC, and PSS-VIC. In this condition, the effect of mechanical generators consisting of three turbines with different time responses, DE, TT, and HT, is not significant due to the total inertia of the system still being sufficient and appropriate to give a counter-torque to dampen the oscillations. This condition is related to the mechanical part of the generators, so PSS has a better power system stability effect than VIC. Therefore, the power system response with VIC only is considered as the base case.

At the high inertia level, the optimal design of PSS-VIC by HHO-MSS offers superior improvement by 41.17% in average frequency nadir reduction of Δf_1, Δf_2, and Δf_{tie} responses compared to the base case. Moreover, the performance indices validation has also justified that PSS-VIC by HHO-MSS has the best average error reduction of 87.05% than the base case. The PSS-VIC design by EEFO, PO, and EMA is the sequence from the second-best to worst after the HHO-MSS. In this simulation, the result by EMA is an example of an inappropriate PSS-VIC design. But, the average error reduction of EMA is still better than the base case. It justifies that the performance indices utilization as constraints formulated in Equation (34) ensures the obtained global parameters of PSS-VIC that reduce the average error from the investigated responses.

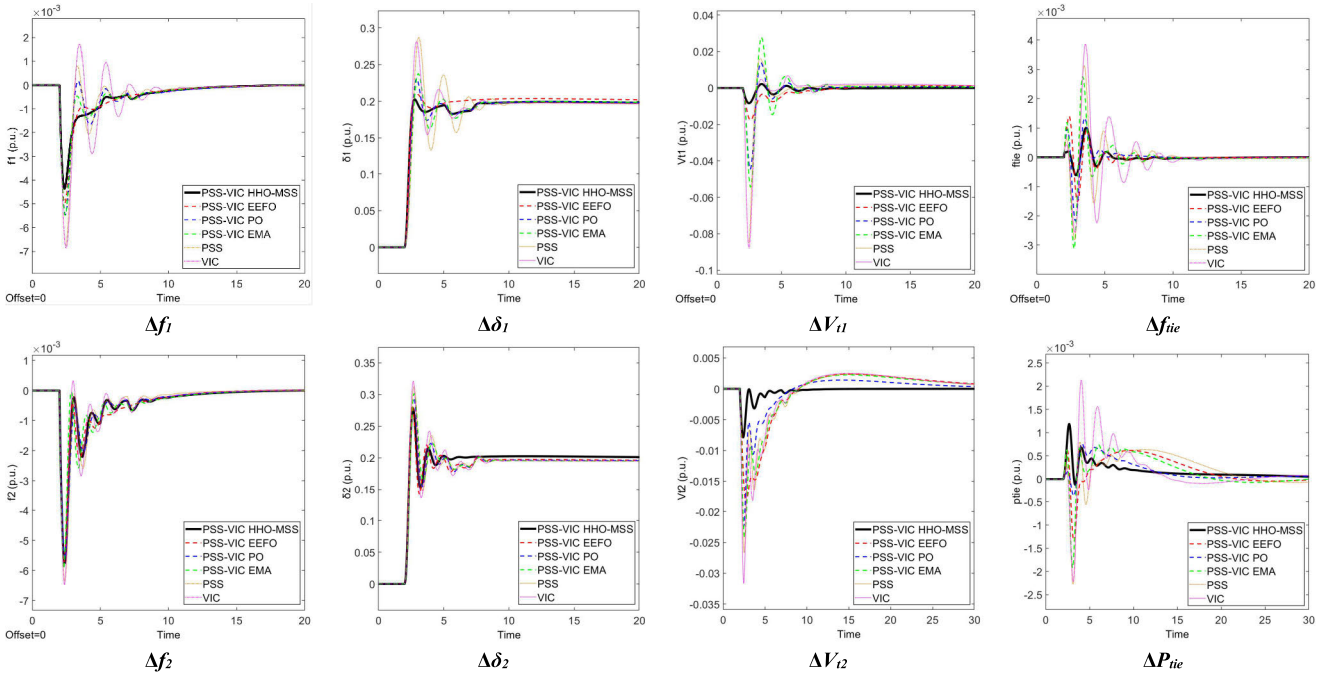

FIGURE 10. Performance of coordinated design of PSS-VIC in Simulation 2: High inertia.

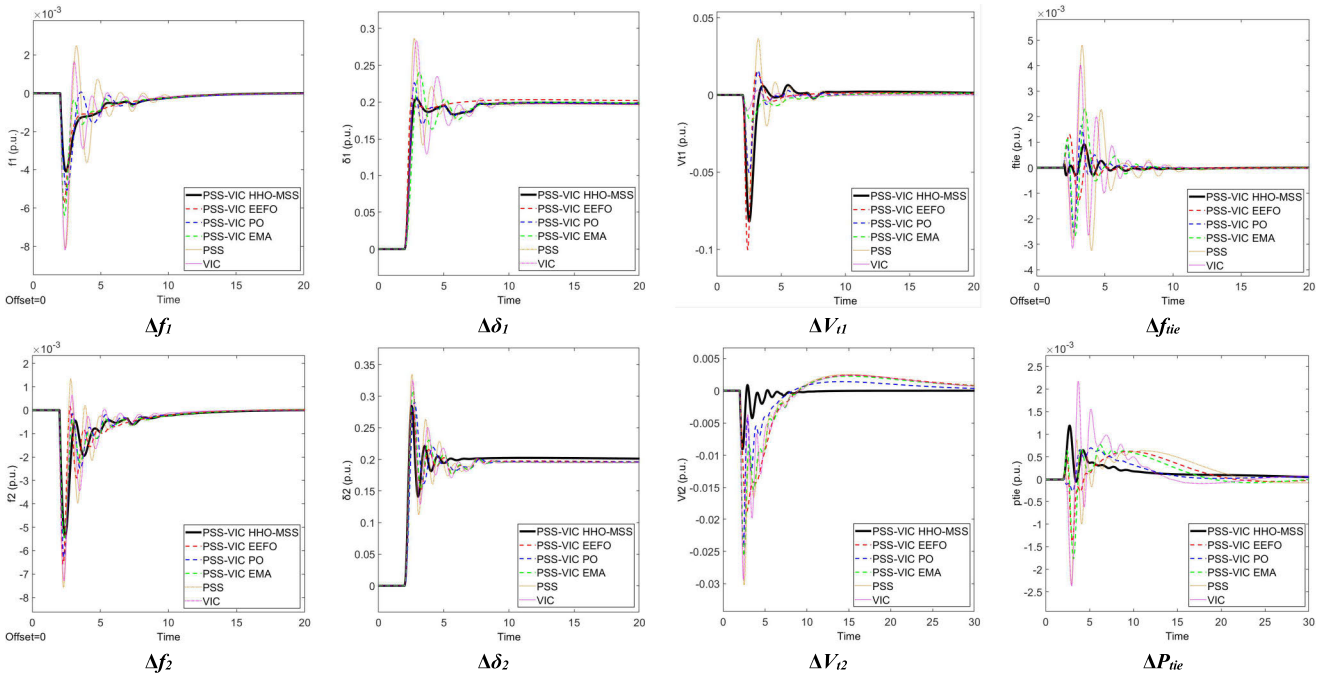

FIGURE 11. Performance of coordinated design of PSS-VIC in Simulation 2: Low inertia.

With the proposed VIC model, the contribution of VIC in improving the power system stability can be clearly investigated at the low inertia level when the power from RES and ESS is sufficient to support the virtual inertia emulation through VIC. At the low inertia level, the total inertia of the system is reduced by 50% ($H_1 = 4.8$, $H_2 = 3.4$), so the natural ability of the system to mitigate the oscillation is also reduced. This condition makes the controller, PSS and VIC, work harder at a low inertia level than high inertia level. Moreover, this power system has three types of turbines with different time responses, so the inertia reduction makes the PSS less effective in dampening the oscillation.

TABLE 11. Frequency nadir comparison of coordinated design of PSS-VIC in Simulation 2: High vs low inertia levels.

Inertia	Controller	Maximum of Frequency Nadir (p.u.)			Improve (%)
		Δf_1	Δf_2	Δf_{tie}	
-20% (high)	VIC	-6.85 x 10^{-3}	-6.47 x 10^{-3}	-2.57 x 10^{-3}	-
	PSS	-6.75 x 10^{-3}	-6.36 x 10^{-3}	-2.82 x 10^{-3}	-2.18
	PSS-VIC HHO-MSS	-4.36 x 10^{-3}	-5.75 x 10^{-3}	-6.16 x 10^{-4}	**41.17**
	PSS-VIC EEFO	-4.97 x 10^{-3}	-5.72 x 10^{-3}	-1.52 x 10^{-3}	26.63
	PSS-VIC PO	-5.46 x 10^{-3}	-5.62 x 10^{-3}	-2.18 x 10^{-3}	16.2
	PSS-VIC EMA	-5.52 x 10^{-3}	-5.93 x 10^{-3}	-3.12 x 10^{-3}	2.12
-50% (low)	PSS	-8.09 x 10^{-3}	-7.57 x 10^{-3}	-3.24 x 10^{-3}	-
	VIC	-8.17 x 10^{-3}	-7.29 x 10^{-3}	-3.16 x 10^{-3}	1.72
	PSS-VIC HHO-MSS	-4.1 x 10^{-3}	-5.4 x 10^{-3}	-3.01 x 10^{-4}	**56.23**
	PSS-VIC EEFO	-5.75 x 10^{-3}	-6.58 x 10^{-3}	-1.32 x 10^{-3}	33.75
	PSS-VIC PO	-5.79 x 10^{-3}	-6.28 x 10^{-3}	-2.54 x 10^{-3}	22.35
	PSS-VIC EMA	-6.37 x 10^{-3}	-5.45 x 10^{-3}	-2.69 x 10^{-3}	22.08

TABLE 12. Performance indices validation of coordinated design of PSS-VIC in Simulation 2: High vs low inertia levels.

Inertia	Controller	Avg. PI = Δf_1, Δf_2, and Δf_{tie}				Avg. Error Reduction (-%)
		ITAE	IAE	ITSE	ISE	
-20% (high)	VIC	3.4 x 10^{-2}	7.09 x 10^{-3}	4.92 x 10^{-5}	1.27 x 10^{-5}	-
	PSS	2.17 x 10^{-2}	4.8 x 10^{-3}	2.67 x 10^{-5}	7.88 x 10^{-6}	38.04
	PSS-VIC HHO-MSS	7.29 x 10^{-3}	1.46 x 10^{-3}	2.32 x 10^{-6}	6.42 x 10^{-7}	**87.05**
	PSS-VIC EEFO	8.25 x 10^{-3}	2.17 x 10^{-3}	5.32 x 10^{-6}	1.79 x 10^{-6}	80.05
	PSS-VIC PO	1.26 x 10^{-2}	2.55 x 10^{-3}	7.94 x 10^{-6}	2.6 x 10^{-6}	72.59
	PSS-VIC EMA	1.82 x 10^{-2}	4.08 x 10^{-3}	2 x 10^{-5}	6.44 x 10^{-6}	49.39
-50% (low)	PSS	3.5 x 10^{-2}	7.49 x 10^{-3}	6.2 x 10^{-5}	1.71 x 10^{-5}	-
	VIC	2.96 x 10^{-2}	6.2 x 10^{-3}	4.05 x 10^{-5}	1.18 x 10^{-5}	26.51
	PSS-VIC HHO-MSS	6.92 x 10^{-3}	1.22 x 10^{-3}	1.57 x 10^{-6}	4.26 x 10^{-7}	**89.73**
	PSS-VIC EEFO	7.61 x 10^{-3}	1.93 x 10^{-3}	4.39 x 10^{-6}	1.48 x 10^{-6}	84.18
	PSS-VIC PO	1.37 x 10^{-2}	2.71 x 10^{-3}	8.85 x 10^{-6}	3.01 x 10^{-6}	73.55
	PSS-VIC EMA	1.91 x 10^{-2}	3.94 x 10^{-3}	1.69 x 10^{-5}	5.26 x 10^{-6}	63.83

From the data, it can be seen that VIC performing better than PSS, thus the PSS is considered as the base case to calculate the improvement percentages. Even so, the frequency nadir is also can be suppressed under 2% (0.02 p.u.) by PSS, VIC, and PSS-VIC. The optimal coordinated design of PSS-VIC by HHO-MSS shows a significant improvement of 56.23% in the average frequency nadir reduction of Δf_1, Δf_2, and Δf_{tie} responses compared to the base case. The performance indices calculation also justifies that the PSS-VIC design by HHO-MSS has the best average error reduction of 89.73% in Δf_1, Δf_2, and Δf_{tie}. The performance of the PSS-VIC design by HHO-MSS is followed by EEFO, PO, and EMA, respectively.

For both high and low inertia levels, the equilibrium points of $\Delta\delta_1$ and $\Delta\delta_2$ shifted to ± 0.2 p.u. due to the low inertia level. From Fig. 11, the optimal design of PSS-VIC by HHO-MSS shows the smoothest and fastest responses in recovering the $\Delta\delta_1$ and $\Delta\delta_2$to the new equilibrium point. In ΔV_{t1},the PSS-VIC design with EMA is better than with HHO-MSS for maintaining voltage stability.However, the PSS-VIC design by HHO-MSS shows superior improvement in ΔV_{t2}over the EEFO, PO, and EMA. Moreover, it can be seen that power transfer between areas oscillates ΔP_{tie}response, and the optimal design of PSS-VIC by HHO-MSS gives significant improvement, followed by PO, EEFO, and EMA.

Based on the result presented in Simulation 2, it can be concluded that PSS-VIC can provide similar performance of power system stability in both high and low inertia, unlike the PSS or VIC alone. The frequency nadir can be suppressed under 2% in both inertia levels, even though the high inertia has better RoCoF than the low inertia ones. Moreover, the optimal design of PSS-VIC by HHO-MSS shows the capability to provide the appropriate amount of additional damping and inertia properties that ensure the power system stability can be similar in various inertia levels, especially in high and low inertia levels.

3) SIMULATION 3: RES LEVEL VARIATION

In this simulation, the adaptivity of PSS-VIC in certain levels of RES is investigated. The simulation scenario in this simulation is arranged based on $\Delta P_{L1} = +0.2$ p.u. and $\Delta P_{L2} = +0.1$ p.u. that occurred at $t_{sim} = 2$ s, followed by $\Delta P_{L1} =$

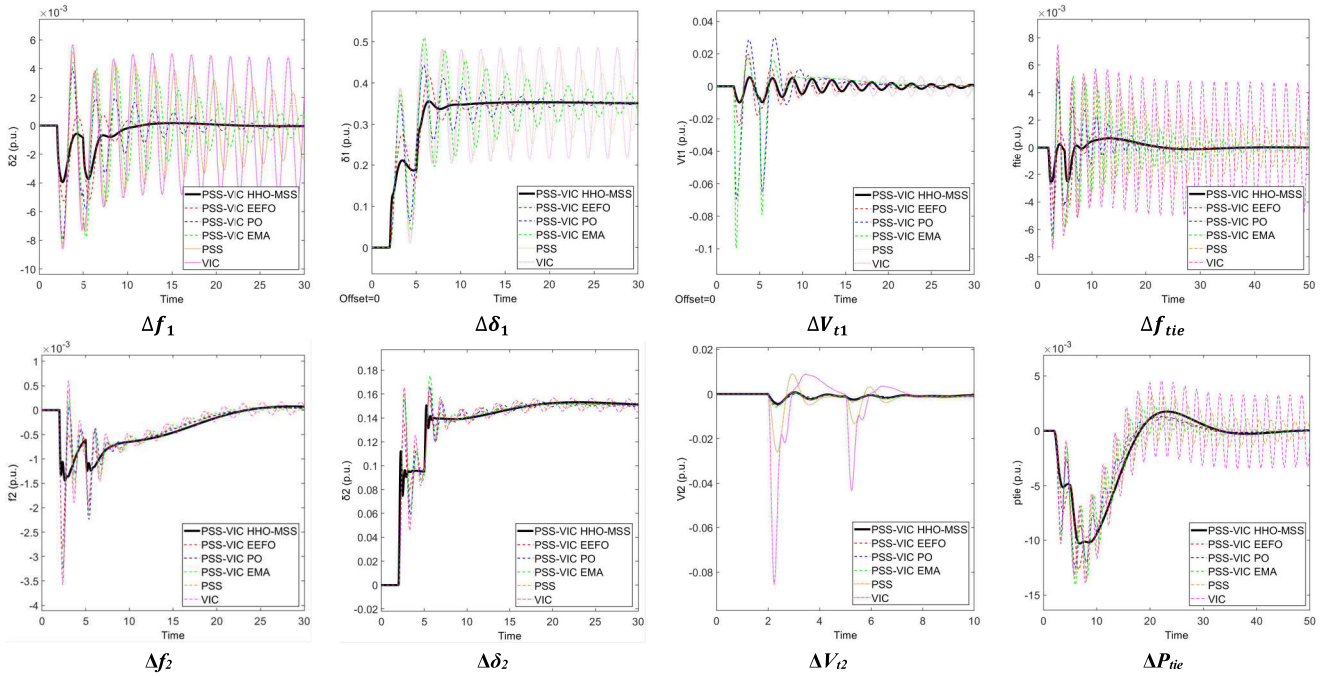

FIGURE 12. Performance of coordinated design of PSS-VIC in Simulation 2: Low RES.

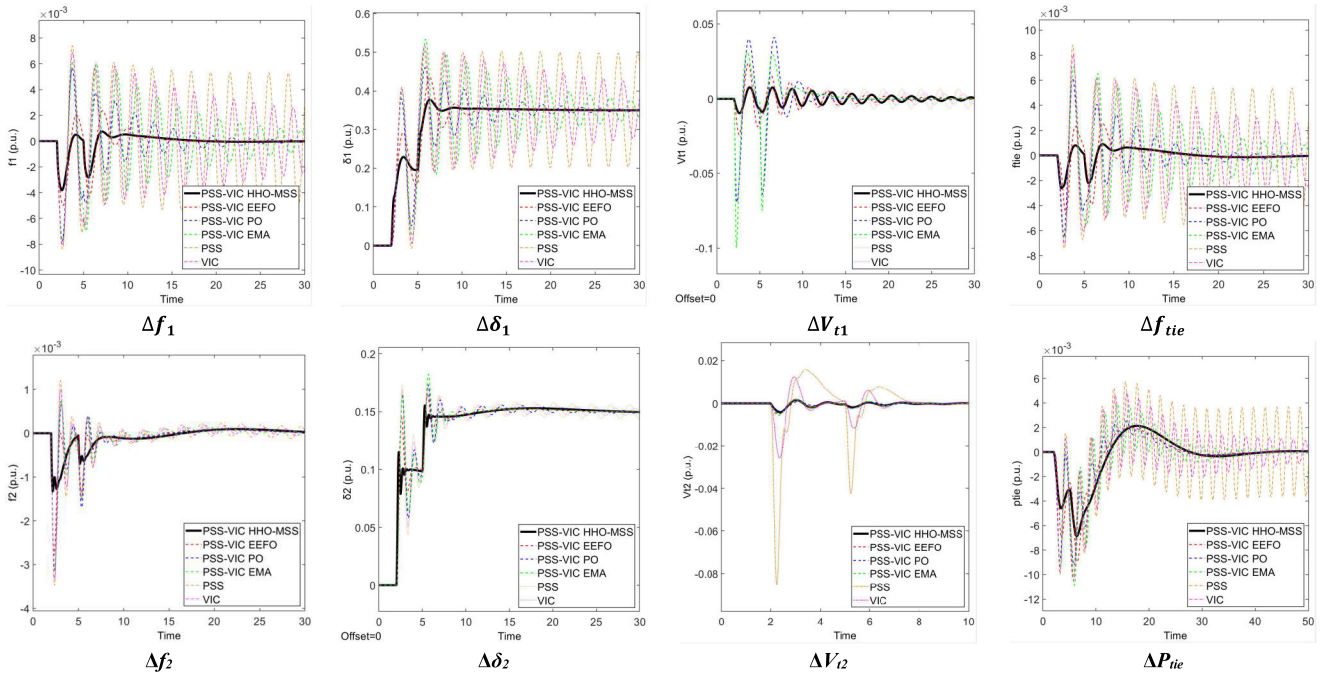

FIGURE 13. Performance of coordinated design of PSS-VIC in Simulation 2: High RES.

+0.015 p.u. and $\Delta P_{L2} = +0.05$ p.u. that occurred at $t_{sim} = 5$ s.

The first scenario assumes a low RES level with 20% of the total supplied power for load demand generated from RES. Thus, the parameters are assumed as follows: 1) At $t_{sim} = 2$ s, $\Delta P_{m1} = +0.16$ p.u., $\Delta P_{m2} = +0.08$ p.u., $\Delta V_{W1} = +0.03$ p.u., $\Delta V_{W2} = +0.015$ p.u., $\Delta\Phi_1 = +0.01$ p.u., and $\Delta\Phi_2 = +0.005$ p.u.; 2) At $t_{sim} = 5$ s, $\Delta P_{m1} = +0.12$ p.u., $\Delta P_{m2} = +0.04$ p.u., $\Delta V_{W1} = +0.02$ p.u., $\Delta V_{W2} = +0.007$ p.u., $\Delta\Phi_1 = +0.01$ p.u., and $\Delta\Phi_2 = +0.003$ p.u. With the proposed virtual inertia emulation model with the proper integration of VIC, RES, and ESS, the

TABLE 13. Statistical Performance of coordinated design of PSS-VIC in Simulation 3: Low vs high RES levels.

RES Level	Controller	Maximum of Frequency Nadir (p.u.)			Improve (%)	Max. Deviation (p.u.)	Improve (%)
		Δf_1	Δf_2	Δf_{tie}		ΔP_{tie}	
20% (low)	VIC	-8.59 x 10^{-3}	-3.58 x 10^{-3}	-7.43 x 10^{-3}	-	-1.39 x 10^{-2}	-
	PSS	-8.31 x 10^{-3}	-3.43 x 10^{-3}	-7.08 x 10^{-3}	4.05	-1.37 x 10^{-2}	1.44
	PSS-VIC HHO-MSS	-3.94 x 10^{-4}	-1.44 x 10^{-3}	-2.54 x 10^{-3}	**70.16**	-1.03 x 10^{-2}	**25.9**
	PSS-VIC EEFO	-5.24 x 10^{-3}	-2.84 x 10^{-3}	-4.62 x 10^{-3}	32.49	-1.27 x 10^{-2}	8.63
	PSS-VIC PO	-7.95 x 10^{-3}	-3.22 x 10^{-3}	-6.52 x 10^{-3}	9.92	-1.25 x 10^{-2}	10.07
	PSS-VIC EMA	-7.89 x 10^{-3}	-3.24 x 10^{-3}	-6.14 x 10^{-3}	11.67	-1.4 x 10^{-2}	-0.72
80% (high)	PSS	-8.38 x 10^{-3}	-3.47 x 10^{-3}	-7.43 x 10^{-3}	-	-1.02 x 10^{-2}	-
	VIC	-8.08 x 10^{-3}	-3.32 x 10^{-3}	-7.08 x 10^{-3}	4.21	-1.05 x 10^{-2}	2.94
	PSS-VIC HHO-MSS	-3.81 x 10^{-3}	-1.33 x 10^{-3}	-2.62 x 10^{-3}	**70.89**	-6.85 x 10^{-3}	**32.84**
	PSS-VIC EEFO	-4.99 x 10^{-3}	-2.78 x 10^{-3}	-4.6 x 10^{-3}	32.8	-8.98 x 10^{-3}	11.96
	PSS-VIC PO	-7.76 x 10^{-3}	-3.11 x 10^{-3}	-6.56 x 10^{-3}	9.83	-9.23 x 10^{-3}	9.51
	PSS-VIC EMA	-7.66 x 10^{-3}	-3.14 x 10^{-3}	-6.59 x 10^{-3}	9.81	-1.08 x 10^{-2}	5.88

TABLE 14. Performance Indices validation of coordinated design of PSS-VIC in Simulation 3: Low vs high RES levels.

RES Level	Controller	Avg. PI = Δf_{tie} and ΔP_{tie}				Avg. Error Reduction (-%)
		ITAE	IAE	ITSE	ISE	
20% (low)	VIC	1.46 x 10^{1}	1.08 x 10^{-1}	7.08 x 10^{-3}	6.45 x 10^{-4}	-
	PSS	1.08 x 10^{0}	9.07 x 10^{-2}	4.93 x 10^{-3}	5.41 x 10^{-4}	22.06
	PSS-VIC HHO-MSS	5.5 x 10^{-1}	5.71 x 10^{-2}	3.04 x 10^{-3}	3.87 x 10^{-4}	**51.57**
	PSS-VIC EEFO	5.93 x 10^{-1}	5.99 x 10^{-2}	3.26 x 10^{-3}	3.97 x 10^{-4}	49.04
	PSS-VIC PO	6.07 x 10^{-1}	6.45 x 10^{-2}	3.2 x 10^{-3}	4.17 x 10^{-4}	47.14
	PSS-VIC EMA	7.98 x 10^{-1}	7.71 x 10^{-2}	3.91 x 10^{-3}	4.83 x 10^{-4}	35.87
80% (high)	PSS	3.68 x 10^{0}	1.52 x 10^{-1}	1.41 x 10^{-2}	5.56 x 10^{-4}	-
	VIC	1.74 x 10^{0}	9.46 x 10^{-2}	4.17 x 10^{-3}	3.44 x 10^{-4}	49.74
	PSS-VIC HHO-MSS	3.17 x 10^{-1}	2.52 x 10^{-2}	7.13 x 10^{-4}	1.04 x 10^{-4}	**87.73**
	PSS-VIC EEFO	3.63 x 10^{-1}	3.58 x 10^{-2}	9.28 x 10^{-4}	1.28 x 10^{-4}	84.24
	PSS-VIC PO	4.23 x 10^{-1}	4.28 x 10^{-2}	1.06 x 10^{-3}	1.64 x 10^{-4}	80.82
	PSS-VIC EMA	8.3 x 10^{-1}	6.3 x 10^{-2}	2.01 x 10^{-3}	2.49 x 10^{-4}	69.24

stability effect given by VIC is less effective than PSS at the low RES level. Thus, the power system stability responses by VIC are considered as the base case. The RES involvement in power systems makes the power system stability worse. From Fig. 12, the critical condition occurred in Area 1 due to it having a bigger RES involvement than Area 2. At the low RES level, the VIC utilization cannot recover quickly the Δf_1 to its steady-state point, while the oscillation still occurred for a long time. The $\Delta\delta_1$ shifted to around +0.35 p.u. and the oscillation was also harder to dampen. This condition can cause an accumulation of oscillations when another disturbance occurs, and the disturbance will spread to the interconnection that can be seen in the Δf_{tie} and ΔP_{tie}. If this condition cannot be mitigated properly, then the blackout will occur. The ineffectiveness of the VIC at the low RES level is caused by the virtual inertia emulation that is related to RES power contribution. Thus, at the low RES level when the mechanical power output is more dominant than RES, PSS becomes more effective than VIC due to the power system stability effect that comes from the mechanical generator scheme. Even though, the PSS only still hard to dampen the oscillation. In Area 2, $\Delta f_2$and $\Delta\delta_2$ are easier to be mitigated, and $\Delta\delta_2$ shifted to around +0.15 p.u.

The PSS-VIC shows a large contribution to the stability improvement. Based on Fig. 12 and Table 13, the optimal design of PSS-VIC by HHO-MSS gives the superior average frequency nadir improvement by 70.16% of Δf_1, Δf_2, and Δf_{tie} responses than the base case. It is followed by EEFO, EMA, and PO. Besides that, the PSS-VIC design by HHO-MSS can dampen the voltage surge in ΔV_{t1} and ΔV_{t2} very well. Moreover, it also offers the best suppression in the maximum deviation in $\Delta P_{tie}$by 25.9% from the base case, which is followed by EEFO and PO. Besides that, the ΔP_{tie}result by EMA shows that the poor PSS-VIC design can lead to the deterioration of the power system stability responses.

The second scenario assumes a high RES level with 80% of the total supplied power for load demand generated from RES. Thus, the parameters are assumed as follows: 1) At t_{sim} = 2 s, ΔP_{m1} = +0.04 p.u., ΔP_{m2} = +0.02 p.u., ΔV_{W1} = +0.1 p.u., ΔV_{W2} = +0.05 p.u., $\Delta\Phi_1$ = +0.06 p.u., and $\Delta\Phi_2$ = +0.03 p.u.; 2) At t_{sim} = 5 s, ΔP_{m1} = +0.3 p.u., ΔP_{m2} = +0.01 p.u., ΔV_{W1} = +0.08 p.u., ΔV_{W2} = +0.03 p.u., $\Delta\Phi_1$ = +0.04 p.u., and $\Delta\Phi_2$ = +0.01 p.u.

Regarding the overall responses, the oscillation that occurred in the second scenario can be dampened better than in the first scenario. It caused by the RES penetration is

actually can increase the power system stability, however the amount and the timing of power injection should be regulated, such as with VIC. With more dominant RES output at the high RES level, the power system stability effect given by VIC is more effective. On the other hand, due to the power generated by mechanical generators being lower than in the first scenario, thus the PSS effect is less effective. Moreover, the mechanical generator consists of three types of turbines with different time responses. Thus, the PSS response is considered as the base case. Similar to the first scenario, the stability of Area 1 is more crucial than Area 2. It can be seen from Fig. 13 that PSS only cannot retain the oscillation in Δf_1 and $\Delta\delta_1$, and it affects the $\Delta f_{tie}$and ΔP_{tie}. The PSS-VIC can sustain the power system stability in ΔV_{t1} and ΔV_{t2}better than PSS or VIC alone.

The detailed statistics at the high RES level are presented in Table 13. The optimal design of PSS-VIC by HHO-MSS has the best improvement of 70.89% of the average frequency nadir reduction in Δf_1, Δf_2, and Δf_{tie}. It can be seen that both in low and high levels of RES, the frequency nadir can be maintained to not exceed the 2% (−0.02 p.u.) of its nominal value. The improvement gap of the obtained results by EEFO, PO, and EMA is very high. It indicates that the PSS-VIC at the high RES level needs to consider the utilized algorithms to maximize the potential stability effect of PSS-VIC. Moreover, the optimal design of PSS-VIC by HHO-MSS also gives a better improvement in $\Delta P_{tie}$of 32.84%. It is followed by EEFO, PO, and EMA.

Table 14 shows that the use of performance indices as optimization constraints guarantees the error reduction of the responses. At the low RES level, the optimal design of PSS-VIC by HHO-MSS achieved the best average error reduction of 51.57%, followed by EEFO, PO, and EMA. While at the high RES level, the optimal design of PSS-VIC by HHO-MSS achieved the best average error reduction of 87.73%, followed by EEFO, PO, and EMA. The tabulated results show that the optimal coordinated design of PSS-VIC with the appropriate addition of damping and inertia keeps the power system stability similar even when the RES level of the system is changed.

V. CONCLUSION

The coordinated design of PSS-VIC for improving power system stability with RES integration by using HHO-MSS is presented. HHO-MSS is used to find the equilibrium point of global parameters of PSS-VIC, which is examined in 38 different simulations based on sudden load changes, different inertia, and RES levels to ensure scalability in power system operating conditions. Moreover, the relationship between RES contribution and VIC effectiveness can be explained with the proposed modification model of VIC.

The statistical assessments of the algorithm performance in PSS-VIC coordination are performed with 30 runs,100 iterations, and 30 search agents. The results show that HHO-MSS is 1.44%, 3.45%, and 9.28% more accurate than EEFO, PO, and EMA, respectively. In addition, HHO-MSS is 34.63%, 48.05%, and 53.94% more consistent than EEFO, PO, and EMA, respectively. Moreover, the convergence curve analysis shows that the HHO is still a feasible option as it can compete with the algorithms that are four to five years newer.

The global parameters of PSS-VIC obtained by HHO-MSS are validated by eigenvalue analysis. The optimal design of PSS-VIC by HHO-MSS offers the best damping ratio in both local and interarea responses which is suitable with grid codes. In the local area response of Area 1, the best damping ratio obtained by HHO-MSS is 9.94%, which is followed by EEFO, PO, and EMA, respectively. In the local area response of Area 2, the best damping ratio obtained by HHO-MSS is 9.95%, which is followed by EEFO, PO, and EMA, respectively. In interarea response, the best damping ratio obtained by HHO-MSS is 9.96%, which is followed by EEFO, PO, and EMA, respectively. The results justify that the HHO-MSS produces the best damping ratio in both local areas and interarea modes. Moreover, the scalability analysis of the PSS-VIC design through the simulations highlights the main finding of this paper in the following:

1) Simulation 1 examines the capability of PSS-VIC to maintain stability under various load changes, including dynamic load. In this simulation, the PSS-VIC provides a better capability than PSS or VIC alone. The optimal design of PSS-VIC by HHO-MSS provides the best stability improvement of 55.29% and 67.38% in $\Delta f_{tie}$and ΔP_{tie}, respectively. It also reduced the settling time by 84.83% to 85.26% in overall responses. Moreover, it produces the best average error reduction ranging from 87.41% to 89.08%. The performance of the optimal deisgn of PSS-VIC by HHO-MSS is followed by EEFO, PO, and EMA.
2) Simulation 2 measures the effectiveness of PSS-VIC in different inertia levels. Based on the results, PSS is more effective than VIC at high inertia level. While VIC gives a better stability effect than PSS at low inertia level. The optimal design of PSS-VIC by HHO-MSS gives the best stability effect indicated by 41.17% and 56.23% frequency nadir improvement of Δf_1, Δf_2, and Δf_{tie} in high and low inertia levels, respectively. Moreover, the optimal design of PSS-VIC by HHO-MSS has also the best average error reduction ranging from 87.05% to 89.73%. It is followed by EEFO, PO, and EMA.
3) Simulation 3 investigates the adaptivity of PSS-VIC in different RES levels. From the obtained results, it can be concluded that PSS performs better than VIC at low RES level, while VIC offers better performance than PSS at high RES level. The optimal design of PSS-VIC by HHO-MSS performs the best frequency nadir improvement of Δf_1, Δf_2, and Δf_{tie} by 70.16% and 70.89% in low and high levels of RES, respec-

tively. It also dampens the oscillation in ΔP_{tie} by 25.9% and 32.84% in low and high levels of RES. Moreover, the performance indices validation shows that the optimal design of PSS-VIC by HHO-MSS gives the best average error reduction ranging from 51.57% to 87.73%.

Based on the simulation and discussion, the proposed approach for finding the optimal coordinated design of PSS-VIC shows excellent performance. Future work will focus on simulating the PSS-VIC in more complex conditions, such as incorporating models of uncertainty and RES fluctuations. The VIC model can also be improved with features to analyze the optimal timing and RES quantity, further improving its implementation effectiveness. Additionally, the PSS and VIC performances should be investigated through experimental methods in future work.

APPENDIX A

$$\dot{\boldsymbol{x}} = \boldsymbol{A}\boldsymbol{x} + \boldsymbol{B}\boldsymbol{u}$$

$$\begin{bmatrix}
\Delta\dot{\delta}_1 \\ \Delta\dot{f}_1 \\ \Delta\dot{P}_{m1} \\ \Delta\dot{P}_{g1} \\ \Delta\dot{P}_{c1} \\ \Delta\dot{P}_{e1} \\ \Delta\dot{E}_{q1} \\ \Delta\dot{E}_{fd1} \\ \Delta\dot{P}_{VI1} \\ \Delta\dot{P}_{WG1} \\ \Delta\dot{P}_{PV1} \\ \Delta\dot{\delta}_2 \\ \Delta\dot{f}_2 \\ \Delta\dot{P}_{m2} \\ \Delta\dot{P}_{g2} \\ \Delta\dot{P}_{c2} \\ \Delta\dot{P}_{e2} \\ \Delta\dot{E}_{q2} \\ \Delta\dot{E}_{fd2} \\ \Delta\dot{P}_{VI2} \\ \Delta\dot{P}_{WG2} \\ \Delta\dot{P}_{PV2}
\end{bmatrix} =
\begin{bmatrix}
f_{R1} & 0 & 0 & 0 & 0 & 0 & 0 & 0 & 0 & 0 & 0 & 0 & 0 & 0 & 0 & 0 & 0 & 0 & 0 & 0 & 0 & 0 & 0 \\
-\frac{T}{2H_1} & -\frac{1}{2H_1} & \frac{1}{2H_1} & 0 & 0 & -\frac{1}{2H_1} & 0 & 0 & \frac{1}{2H_1} & \frac{1}{2H_1} & \frac{1}{2H_1} & \frac{1}{2H_1} & 0 & 0 & 0 & 0 & 0 & 0 & 0 & 0 & 0 & 0 & 0 \\
0 & 0 & 0 & \frac{1}{Tg_1} & 0 & 0 & 0 & 0 & 0 & 0 & 0 & 0 & 0 & 0 & 0 & 0 & 0 & 0 & 0 & 0 & 0 & 0 & 0 \\
0 & \frac{1}{R_{D1}Tg_1} & 0 & \frac{1}{Tg_1} & \frac{1}{Tg_1} & 0 & 0 & 0 & 0 & 0 & 0 & 0 & 0 & 0 & 0 & 0 & 0 & 0 & 0 & 0 & 0 & 0 & 0 \\
0 & K_{s1}\beta_1 & 0 & 0 & 0 & 0 & 0 & 0 & 0 & 0 & 0 & 0 & 0 & 0 & 0 & 0 & 0 & 0 & 0 & 0 & 0 & 0 & 0 \\
-\frac{K_{11}}{2H_1} & -\frac{D_1}{2H_1} & 0 & 0 & 0 & 0 & -\frac{K_{21}}{2H_1} & 0 & 0 & 0 & 0 & 0 & 0 & 0 & 0 & 0 & 0 & 0 & 0 & 0 & 0 & 0 & 0 \\
-\frac{K_{41}}{T_{ex1}} & 0 & 0 & 0 & 0 & 0 & -\frac{1}{T_{ex1}K_{31}} & \frac{1}{T_{ex1}} & 0 & 0 & 0 & 0 & 0 & 0 & 0 & 0 & 0 & 0 & 0 & 0 & 0 & 0 & 0 \\
\frac{k_{a1}K_{51}}{T_{a1}} & -\frac{k_{a1}K_{61}}{T_{a1}} & 0 & 0 & 0 & 0 & 0 & \frac{1}{T_{a1}} & 0 & 0 & 0 & 0 & 0 & 0 & 0 & 0 & 0 & 0 & 0 & 0 & 0 & 0 & 0 \\
0 & 0 & 0 & 0 & 0 & 0 & 0 & 0 & -\frac{1}{T_{INV1}} & \frac{1}{T_{WG1}T_{INV21}} & \frac{1}{T_{PV1}T_{INV31}} & 0 & 0 & 0 & 0 & 0 & 0 & 0 & 0 & 0 & 0 & 0 & 0 \\
0 & 0 & 0 & 0 & 0 & 0 & 0 & 0 & 0 & -\frac{1}{T_{WG1}T_{INV21}} & 0 & 0 & 0 & 0 & 0 & 0 & 0 & 0 & 0 & 0 & 0 & 0 & 0 \\
0 & 0 & 0 & 0 & 0 & 0 & 0 & 0 & 0 & 0 & -\frac{1}{T_{PV1}T_{INV31}} & 0 & 0 & 0 & 0 & 0 & 0 & 0 & 0 & 0 & 0 & 0 & 0 \\
0 & 0 & 0 & 0 & 0 & 0 & 0 & 0 & 0 & 0 & 0 & 0 & f_{R2} & 0 & 0 & 0 & 0 & 0 & 0 & 0 & 0 & 0 & 0 \\
\frac{T}{2H_2} & 0 & 0 & 0 & 0 & 0 & 0 & 0 & 0 & 0 & 0 & 0 & \frac{T}{2H_2} & -\frac{1}{2H_2} & \frac{1}{2H_2} & 0 & 0 & -\frac{1}{2H_2} & 0 & 0 & \frac{1}{2H_2} & \frac{1}{2H_2} & \frac{1}{2H_2} \\
0 & 0 & 0 & 0 & 0 & 0 & 0 & 0 & 0 & 0 & 0 & 0 & 0 & 0 & 0 & \frac{1}{Tg_2} & 0 & 0 & 0 & 0 & 0 & 0 & 0 \\
0 & 0 & 0 & 0 & 0 & 0 & 0 & 0 & 0 & 0 & 0 & 0 & 0 & \frac{1}{R_{D2}Tg_2} & 0 & \frac{1}{Tg_2} & \frac{1}{Tg_2} & 0 & 0 & 0 & 0 & 0 & 0 \\
0 & 0 & 0 & 0 & 0 & 0 & 0 & 0 & 0 & 0 & 0 & 0 & 0 & K_{s2}\beta_2 & 0 & 0 & 0 & 0 & 0 & 0 & 0 & 0 & 0 \\
0 & 0 & 0 & 0 & 0 & 0 & 0 & 0 & 0 & 0 & 0 & 0 & -\frac{K_{12}}{2H_2} & -\frac{D_2}{2H_2} & 0 & 0 & 0 & -\frac{K_{22}}{2H_2} & 0 & 0 & 0 & 0 & 0 \\
0 & 0 & 0 & 0 & 0 & 0 & 0 & 0 & 0 & 0 & 0 & 0 & -\frac{K_{42}}{T_{ex2}} & 0 & 0 & 0 & 0 & -\frac{1}{T_{ex2}K_{32}} & \frac{1}{T_{ex2}} & 0 & 0 & 0 & 0 \\
0 & 0 & 0 & 0 & 0 & 0 & 0 & 0 & 0 & 0 & 0 & 0 & \frac{k_{a2}K_{52}}{T_{a2}} & -\frac{k_{a2}K_{62}}{T_{a2}} & 0 & 0 & 0 & 0 & \frac{1}{T_{a2}} & 0 & 0 & 0 & 0 \\
0 & 0 & 0 & 0 & 0 & 0 & 0 & 0 & 0 & 0 & 0 & 0 & 0 & 0 & 0 & 0 & 0 & 0 & 0 & -\frac{1}{T_{INV2}} & \frac{1}{T_{WG2}T_{INV22}} & \frac{1}{T_{PV2}T_{INV32}} & 0 \\
0 & 0 & 0 & 0 & 0 & 0 & 0 & 0 & 0 & 0 & 0 & 0 & 0 & 0 & 0 & 0 & 0 & 0 & 0 & 0 & -\frac{1}{T_{WG2}T_{INV22}} & 0 & 0 \\
0 & 0 & 0 & 0 & 0 & 0 & 0 & 0 & 0 & 0 & 0 & 0 & 0 & 0 & 0 & 0 & 0 & 0 & 0 & 0 & 0 & -\frac{1}{T_{PV2}T_{INV32}} & 0
\end{bmatrix}
\begin{bmatrix}
\Delta\delta_1 \\ \Delta f_1 \\ \Delta P_{m1} \\ \Delta P_{g1} \\ \Delta P_{c1} \\ \Delta P_{e1} \\ \Delta E_{q1} \\ \Delta E_{fd1} \\ \Delta P_{VI1} \\ \Delta P_{WG1} \\ \Delta P_{PV1} \\ \Delta\delta_2 \\ \Delta f_2 \\ \Delta P_{m2} \\ \Delta P_{g2} \\ \Delta P_{c2} \\ \Delta P_{e2} \\ \Delta E_{q2} \\ \Delta E_{fd2} \\ \Delta P_{VI2} \\ \Delta P_{WG2} \\ \Delta P_{PV2}
\end{bmatrix}$$

$$+
\begin{bmatrix}
0 & 0 & 0 & 0 & 0 & 0 & 0 & 0 & 0 & 0 & 0 & 0 & 0 & 0 & 0 & 0 \\
-\frac{1}{2H_1} & 0 & 0 & 0 & 0 & 0 & 0 & 0 & 0 & 0 & 0 & 0 & 0 & 0 & 0 & 0 \\
0 & 0 & 0 & 0 & 0 & 0 & 0 & 0 & 0 & 0 & 0 & 0 & 0 & 0 & 0 & 0 \\
0 & -\frac{1}{Tg_1} & 0 & 0 & 0 & 0 & 0 & 0 & 0 & 0 & 0 & 0 & 0 & 0 & 0 & 0 \\
0 & 0 & 0 & 0 & 0 & 0 & 0 & 0 & 0 & 0 & 0 & 0 & 0 & 0 & 0 & 0 \\
0 & 0 & 0 & 0 & 0 & 0 & 0 & 0 & 0 & 0 & 0 & 0 & 0 & 0 & 0 & 0 \\
0 & 0 & -\frac{k_{a1}}{T_{a1}} & 0 & 0 & 0 & 0 & 0 & 0 & 0 & 0 & 0 & 0 & 0 & 0 & 0 \\
0 & 0 & 0 & \frac{1}{R_{VI1}T_{ESS1}T_{INV11}} & \frac{1}{R_{VI1}T_{ESS1}T_{INV11}} & 0 & 0 & 0 & 0 & 0 & 0 & 0 & 0 & 0 & 0 & 0 \\
0 & 0 & 0 & 0 & 0 & \frac{1}{T_{WG1}T_{INV21}} & 0 & 0 & 0 & 0 & 0 & 0 & 0 & 0 & 0 & 0 \\
0 & 0 & 0 & 0 & 0 & 0 & \frac{1}{T_{PV1}T_{INV31}} & 0 & 0 & 0 & 0 & 0 & 0 & 0 & 0 & 0 \\
0 & 0 & 0 & 0 & 0 & 0 & 0 & 0 & 0 & 0 & 0 & 0 & 0 & 0 & 0 & 0 \\
0 & 0 & 0 & 0 & 0 & 0 & 0 & -\frac{1}{2H_2} & 0 & 0 & 0 & 0 & 0 & 0 & 0 & 0 \\
0 & 0 & 0 & 0 & 0 & 0 & 0 & 0 & -\frac{1}{Tg_2} & 0 & 0 & 0 & 0 & 0 & 0 & 0 \\
0 & 0 & 0 & 0 & 0 & 0 & 0 & 0 & 0 & 0 & 0 & 0 & 0 & 0 & 0 & 0 \\
0 & 0 & 0 & 0 & 0 & 0 & 0 & 0 & 0 & 0 & 0 & 0 & 0 & 0 & 0 & 0 \\
0 & 0 & 0 & 0 & 0 & 0 & 0 & 0 & 0 & 0 & 0 & 0 & 0 & 0 & 0 & 0 \\
0 & 0 & 0 & 0 & 0 & 0 & 0 & 0 & -\frac{k_{a2}}{T_{a2}} & 0 & 0 & 0 & 0 & 0 & 0 & 0 \\
0 & 0 & 0 & 0 & 0 & 0 & 0 & 0 & 0 & \frac{1}{R_{VI2}T_{ESS2}T_{INV12}} & \frac{1}{R_{VI2}T_{ESS2}T_{INV12}} & 0 & 0 & 0 & 0 & 0 \\
0 & 0 & 0 & 0 & 0 & 0 & 0 & 0 & 0 & 0 & 0 & \frac{1}{T_{WG2}T_{INV22}} & 0 & 0 & 0 & 0 \\
0 & 0 & 0 & 0 & 0 & 0 & 0 & 0 & 0 & 0 & 0 & 0 & \frac{1}{T_{PV2}T_{INV32}} & 0 & 0 & 0
\end{bmatrix}
\begin{bmatrix}
\Delta P_{L1} \\ \Delta P_{M1} \\ \Delta V_{PSS1} \\ \Delta D_{VI1} \\ \Delta K_{VI1} \\ \Delta V_{W1} \\ \Delta \Phi_1 \\ \Delta P_{L2} \\ \Delta P_{M2} \\ \Delta V_{PSS2} \\ \Delta D_{VI2} \\ \Delta K_{VI2} \\ \Delta V_{W2} \\ \Delta \Phi_2
\end{bmatrix}$$

ACKNOWLEDGMENT

The authors would like to express their gratitude to the members of the Power System Operation and Control (PSOC) Research Group, Power System Simulation Laboratory (PSSL), and PMDSU Batch VI Scholarship, who always supported them in the research and writing process. This research was conducted during the Inbound Researcher Mobility (IRM) ITS 2024 Program, that accommodated Prof. Alberto Borghetti as a Guest Professor with ITS, Surabaya, Indonesia.

REFERENCES

[1] M. S. Alvarez-Alvarado, D. L. Donaldson, A. A. Recalde, H. H. Noriega, Z. A. Khan, W. Velasquez, and C. D. Rodríguez-Gallegos, "Power system reliability and maintenance evolution: A critical review and future perspectives," *IEEE Access*, vol. 10, pp. 51922–51950, 2022, doi: 10.1109/ACCESS.2022.3172697.

[2] C. Wang, P. Ju, F. Wu, X. Pan, and Z. Wang, "A systematic review on power system resilience from the perspective of generation, network, and load," *Renew. Sustain. Energy Rev.*, vol. 167, Oct. 2022, Art. no. 112567, doi: 10.1016/j.rser.2022.112567.

[3] S. Mehta and P. Basak, "A comprehensive review on control techniques for stability improvement in microgrids," *Int. Trans. Electr. Energy Syst.*, vol. 31, no. 4, pp. 1–28, Apr. 2021, doi: 10.1002/2050-7038.12822.

[4] N. Hatziargyriou, J. Milanovic, C. Rahmann, V. Ajjarapu, C. Canizares, I. Erlich, D. Hill, I. Hiskens, I. Kamwa, B. Pal, P. Pourbeik, J. Sanchez-Gasca, A. Stankovic, T. Van Cutsem, V. Vittal, and C. Vournas, "Definition and classification of power system stability–revisited & extended," *IEEE Trans. Power Syst.*, vol. 36, no. 4, pp. 3271–3281, Jul. 2021, doi: 10.1109/TPWRS.2020.3041774.

[5] P. S. Kundur and O. P. Malik, *Power System Stability and Control*, 2nd ed., New York, NY, USA: McGraw-Hill, 2020.

[6] A. B. Kunya, M. Argin, Y. Jibril, and Y. A. Shaaban, "Improved model predictive load frequency control of interconnected power system with synchronized automatic generation control loops," *Beni-Suef Univ. J. Basic Appl. Sci.*, vol. 9, no. 1, pp. 1–13, Dec. 2020, doi: 10.1186/s43088-020-00072-w.

[7] A. Nocoń and S. Paszek, "A comprehensive review of power system stabilizers," *Energies*, vol. 16, no. 4, p. 1945, Feb. 2023, doi: 10.3390/en16041945.

[8] M. Izdebski, R. Małkowski, and P. Miller, "New performance indices for power system stabilizers," *Energies*, vol. 15, no. 24, p. 9582, Dec. 2022, doi: 10.3390/en15249582.

[9] R. Rajbongshi, L. C. Saikia, W. Tasnin, A. Saha, and D. Saha, "Performance analysis of combined ALFC and AVR system incorporating power system stabilizer," in *Proc. 2nd Int. Conf. Energy, Power Environ. Towar. Smart Technol. (ICEPE)*, 2018, pp. 1–6, doi: 10.1109/EPETSG.2018.8658874.

[10] E. Jamil, S. Hameed, R. K. Pachauri, B. Khan, and A. A. Ali, "Mitigation of power system oscillations in wind farm integrated multi-machine system using PSS and TCSC," *Wind Energ. Sci. Discuss.*, 2024, doi: 10.5194/wes-2024-75.

[11] P. He, Q. Fang, H. Jin, Y. Ji, Z. Gong, and J. Dong, "Coordinated design of PSS and STATCOM-POD based on the GA-PSO algorithm to improve the stability of wind-PV-thermal-bundled power system," *Int. J. Electr. Power Energy Syst.*, vol. 141, Oct. 2022, Art. no. 108208, doi: 10.1016/j.ijepes.2022.108208.

[12] A. Kumar, A. K. Chandel, and S. Tiwari, "Transient stability improvement of multi-machine system by using STATCOM with power system stabilizer," in *Proc. IEEE Int. Students' Conf. Elect., Electron. Comput. Sci. (SCEECS)*, 2024, pp. 1–5, doi: 10.1109/SCEECS61402.2024.10482178.

[13] S. K. Barik and S. K. Mohapatra, "Coordinated control of multi band PSS (MBPSS) with type 2 fuzzy based SSSC controller design for power system stability improvement," *Evol. Intell.*, vol. 17, no. 3, pp. 1909–1932, Jun. 2024, doi: 10.1007/s12065-023-00871-x.

[14] S. Satheesan and T. T. Anilkumar, "Coordinated control of PSS and SSSC using ant colony optimization," in *Proc. Int. Conf. Advancements Power, Commun. Intell. Syst. (APCI)*, Jun. 2024, pp. 1–6, doi: 10.1109/apci61480.2024.10616952.

[15] N. M. A. Ibrahim, E. A. El-said, H. E. M. Attia, and B. A. Hemade, "Enhancing power system stability: An innovative approach using coordination of FOPID controller for PSS and SVC FACTS device with MFO algorithm," *Electr. Eng.*, vol. 106, no. 3, pp. 2265–2283, Jun. 2024, doi: 10.1007/s00202-023-02051-7.

[16] M. A. Ayaz, I. Ahmad Khan, and S. Rahman, "Intelligent damping of low-frequency oscillations in solar integrated power systems using ANFIS-based SVC control," in *Proc. IEEE Int. Conf. Energy Technol. Futur. Grids (ETFG)*, Feb. 2023, pp. 1–6, doi: 10.1109/ETFG55873.2023.10408369.

[17] S. Choudhury, N. Khandelwal, and T. P. Dash, "A unified scheme of PSS and SVC for voltage profile improvement in electrical grid network," in *Proc. 1st Odisha Int. Conf. Electr. Power Eng., Commun. Comput. Technol. (ODICON)*, Jan. 2021, pp. 1–6, doi: 10.1109/ODICON50556.2021.9428989.

[18] A. Toolabi Moghadam, M. Aghahadi, M. Eslami, S. Rashidi, B. Arandian, and S. Nikolovski, "Adaptive rat swarm optimization for optimum tuning of SVC and PSS in a power system," *Int. Trans. Electr. Energy Syst.*, vol. 2022, pp. 1–13, Jan. 2022, doi: 10.1155/2022/4798029.

[19] X. Wang and Y. Zhou, "Optimization design of PSS and SVC coordination controller based on the neighborhood rough set and improved whale optimization algorithm," *Electronics*, vol. 13, no. 12, p. 2300, Jun. 2024, doi: 10.3390/electronics13122300.

[20] M. R. Djalal, I. Robandi, and M. A. Prakasa, "Stability enhancement of sulselrabar electricity system using mayfly algorithm based on static var compensator and multi-band power system stabilizer PSS2B," *IEEE Access*, vol. 11, pp. 57319–57340, 2023, doi: 10.1109/ACCESS.2023.3283598.

[21] M. A. Prakasa, I. Robandi, R. Nishimura, and M. R. Djalal, "A new scheme of Harris hawk optimizer with memory saving strategy (HHO-MSS) for controlling parameters of power system stabilizer and virtual inertia in renewable microgrid power system," *IEEE Access*, vol. 12, pp. 73849–73878, 2024, doi: 10.1109/ACCESS.2024.3385089.

[22] M. A. Prakasa, I. Robandi, R. Nishimura, and M. R. Djalal, "A hybrid controlling parameters of power system stabilizer and virtual inertia using Harris hawk optimizer in interconnected renewable power systems," *IEEE Access*, vol. 12, pp. 76219–76243, 2024, doi: 10.1109/ACCESS.2024.3405994.

[23] T. Kerdphol, F. S. Rahman, M. Watanabe, and Y. Mitani. (2021). *Virtual Inertia Synthesis and Control*. [Online]. Available: https://link.springer.com/book/10.1007/978-3-030-57961-60Ahttp://link.springer.com/10.1007/978-3-030-57961-6

[24] A. Altaf, M. Kumar, D. Biswas, R. Mahadeva, and S. P. Patole, "Virtual inertia controller design based on mixed sensitivity constraint H∞ approach for load frequency regulation of islanded AC microgrid," *IEEE Access*, vol. 12, pp. 102328–102336, 2024, doi: 10.1109/ACCESS.2024.3433027.

[25] M. A. Shobug, N. A. Chowdhury, M. A. Hossain, M. J. Sanjari, J. Lu, and F. Yang, "Virtual inertia control for power electronics-integrated power systems: Challenges and prospects," *Energies*, vol. 17, no. 11, p. 2737, Jun. 2024, doi: 10.3390/en17112737.

[26] V. Skiparev, R. Machlev, N. R. Chowdhury, Y. Levron, E. Petlenkov, and J. Belikov, "Virtual inertia control methods in islanded microgrids," *Energies*, vol. 14, no. 6, p. 1562, Mar. 2021, doi: 10.3390/en14061562.

[27] L. Yathisha and S. Patilkulkarni, "LQR and LQG based optimal switching techniques for PSS and UPFC in power systems," *Control Theory Technol.*, vol. 16, no. 1, pp. 25–37, Feb. 2018, doi: 10.1007/s11768-018-6174-x.

[28] D. Acharya and D. K. Das, "An optimal membership function based fuzzy-PIλ stabilizer design to suppress low frequency oscillation in synchronous generator," *Results Control Optim.*, vol. 14, Mar. 2024, Art. no. 100374, doi: 10.1016/j.rico.2024.100374.

[29] P. C. Sahu, "Impact and integration of electric vehicles on renewable energy based microgrid: Frequency profile improvement by a-SCA optimized FO-fuzzy PSS approach," *Green Energy Intell. Transp.*, 2024, Art. no. 100191, doi: 10.1016/j.geits.2024.100191.

[30] M. Saini and A. M. S. Yunus, "Design of a robust PID-PSS & FACTS using craziness particle swarm optimization in sulselrabar system," *Int. J. Intell. Eng. Syst.*, vol. 17, no. 4, pp. 491–503, 2024, doi: 10.22266/ijies2024.0831.38.

[31] K. Hongesombut and R. Keteruksa, "Fractional order based on a flower pollination algorithm PID controller and virtual inertia control for microgrid frequency stabilization," *Electric Power Syst. Res.*, vol. 220, Jul. 2023, Art. no. 109381, doi: 10.1016/j.epsr.2023.109381.

[32] M. A. Afifi, M. I. Marei, and A. M. I. Mohamad, "Reinforcement-Learning-Based virtual inertia controller for frequency support in islanded microgrids," *Technologies*, vol. 12, no. 3, p. 39, Mar. 2024, doi: 10.3390/technologies12030039.

[33] K. Y. Yap, C. R. Sarimuthu, and J. M. Lim, "Grid integration of solar photovoltaic system using machine learning-based virtual inertia synthetization in synchronverter," *IEEE Access*, vol. 8, pp. 49961–49976, 2020, doi: 10.1109/ACCESS.2020.2980187.

[34] V. Skiparev, K. Nosrati, A. Tepljakov, E. Petlenkov, Y. Levron, J. Belikov, and J. M. Guerrero, "Virtual inertia control of isolated microgrids using an NN-based VFOPID controller," *IEEE Trans. Sustain. Energy*, vol. 14, no. 3, pp. 1558–1568, Jan. 2023, doi: 10.1109/TSTE.2023.3237922.
[35] D. U. Sarkar and T. Prakash, "A convolutional neural network framework to design power system stabilizer for damping oscillations in multi-machine power system," *Neural Comput. Appl.*, vol. 36, no. 9, pp. 5059–5075, Mar. 2024, doi: 10.1007/s00521-023-09323-0.
[36] A. O. Aluko, D. G. Dorrell, R. Pillay Carpanen, and E. E. Ojo, "Heuristic optimization of virtual inertia control in grid-connected wind energy conversion systems for frequency support in a restructured environment," *Energies*, vol. 13, no. 3, p. 564, Jan. 2020, doi: 10.3390/en13030564.
[37] A. Pratap, S. K. Sharma, and A. Khandelwal, "A review of modern virtual inertia control strategies for microgrid implementation," in *Proc. IEEE 2nd Int. Conf. Electr. Power Energy Syst. (ICEPES)*, Dec. 2021, pp. 1–6, doi: 10.1109/ICEPES52894.2021.9699804.
[38] M. A. Prakasa and I. Robandi, "Tuning improvement of power system stabilizer using hybrid Harris hawk optimization-equilibrium optimizer algorithm," in *Proc. 6th Int. Conf. Inf. Technol., Inf. Syst. Electr. Eng. (ICITISEE)*, Dec. 2022, pp. 553–558.
[39] M. A. Prakasa and I. Robandi, "Optimal tuning for power system stabilizer using arithmetic optimizer algorithm in interconnected two-area power system," in *Proc. Int. Seminar Intell. Technol. Appl. (ISITIA)*, Jul. 2023, pp. 798–803, doi: 10.1109/isitia59021.2023.10221034.
[40] M. R. Djalal, I. Robandi, and M. A. Prakasa, "Stability improvement of sulselrabar system with integrated wind power plant using multi-band PSS3C based mayfly optimization algorithm," *IEEE Access*, vol. 12, pp. 76707–76734, 2024, doi: 10.1109/ACCESS.2024.3406434.
[41] L. Chaib, A. Choucha, S. Arif, H. G. Zaini, A. El-Fergany, and S. S. M. Ghoneim, "Robust design of power system stabilizers using improved Harris hawk optimizer for interconnected power system," *Sustainability*, vol. 13, no. 21, p. 11776, Oct. 2021, doi: 10.3390/su132111776.
[42] R. Devarapalli, N. K. Sinha, and F. P. García Márquez, "A review on the computational methods of power system stabilizer for damping power network oscillations," *Arch. Comput. Methods Eng.*, vol. 29, no. 6, pp. 3713–3739, Oct. 2022, doi: 10.1007/s11831-022-09712-z.
[43] M. H. Sulaiman, Z. Mustaffa, M. M. Saari, H. Daniyal, and S. Mirjalili, "Evolutionary mating algorithm," *Neural Comput. Appl.*, vol. 35, no. 1, pp. 487–516, Jan. 2023, doi: 10.1007/s00521-022-07761-w.
[44] W. Zhao, L. Wang, Z. Zhang, H. Fan, J. Zhang, S. Mirjalili, N. Khodadadi, and Q. Cao, "Electric eel foraging optimization: A new bio-inspired optimizer for engineering applications," *Expert Syst. Appl.*, vol. 238, Mar. 2024, Art. no. 122200, doi: 10.1016/j.eswa.2023.122200.
[45] B. Abdollahzadeh, N. Khodadadi, S. Barshandeh, P. Trojovský, F. S. Gharehchopogh, E.-S.-M. El-kenawy, L. Abualigah, and S. Mirjalili, "Puma optimizer (PO): A novel metaheuristic optimization algorithm and its application in machine learning," *Cluster Comput.*, vol. 27, no. 4, pp. 5235–5283, Jul. 2024, doi: 10.1007/s10586-023-04221-5.
[46] *IEEE Recommended Practice for Excitation System Models for Power System Stability Studies*, IEEE Standard 421.5-2016 (Revision of IEEE Std 421.5-2005), pp. 1–207, Aug. 2016, doi: 10.1109/IEEESTD.2016.7553421.
[47] M. Energi and M. S. Daya, "Aturan jaringan sistem tenaga listrik (indonesian grid code)," Ministry Energy Mineral Resour. Indonesian Republic, 2020.
[48] A. A. Heidari, S. Mirjalili, H. Faris, I. Aljarah, M. Mafarja, and H. Chen, "Harris hawks optimization: Algorithm and applications," *Future Gener. Comput. Syst.*, vol. 97, pp. 849–872, Aug. 2019, doi: 10.1016/j.future.2019.02.028.

MOHAMAD ALMAS PRAKASA was born in Brebes, Indonesia, in September 1999. He received the bachelor's degree from the Department of Electrical Engineering, Universitas Negeri Semarang (UNNES), Semarang, Indonesia, in 2021, and the master's degree from the Department of Electrical Engineering, Institut Teknologi Sepuluh Nopember (ITS), Surabaya, Indonesia, in 2023, where he is currently pursuing the Ph.D. degree. He received the PMDSU Batch VI Scholarship (fast-track program) from the Indonesian government. He is a member of the Power System Operation and Control (PSOC) Research Group, Power System Simulation Laboratory (PSSL). He is interested in artificial intelligence applications for electrical power and energy systems.

IMAM ROBANDI was born in Central Java, Indonesia. He received the Bachelor of Engineering degree from the Institut Teknologi Sepuluh Nopember (ITS), in 1989, the master's degree from the Institut Teknologi Bandung (ITB), Indonesia, in 1995, and the Dr.-Eng. (Doctor of Engineering) degree from Tottori University, Japan, in 2002. He has been a Visiting Professor with several universities in Japan. He is currently carry out research in the area of large-scale electric power systems and artificial intelligence applications for energy control in electric vehicle. He is currently working on several researches with national research grants. He is also the Head of the ITS Professor Council and the Deputy of the Indonesian Professors Association and the Indonesian Professors Council Forum.

ALBERTO BORGHETTI was born in Cesena, Italy, in 1967. He received the Laurea degree (Hons.) in electrical engineering from the University of Bologna, Bologna, Italy, in 1992. Since then, he has been with the Power System Group, University of Bologna, where he is currently a Professor of electrical power systems. His research interests include power system analysis, power system restoration after blackout, electromagnetic transients, optimal generation scheduling, and distribution system operation. He was a recipient of the International Conference on Lightning Protection (ICLP) Scientific Committee Award, in 2016, and the 2018 CIGRE Technical Council Award for SC C4 (System Technical Performance). From 2010 to 2017, he was an Associate Editor of IEEE Transactions on Smart Grids, from 2018 to 2022; and an Associate Editor of IEEE Transactions on Power Systems, from January 2019 to February 2023. He served as the Editor-in-Chief for *Electrical Engineering–Archiv fur Elektrotechnik*.

MUHAMMAD RUSWANDI DJALAL was born in Ujung Pandang, Indonesia, in March 1990. He received the bachelor's degree in energy engineering from Politeknik Negeri Ujung Pandang, Makassar, Indonesia, in 2012, and the master's degree from the Department of Electrical Engineering, Institut Teknologi Sepuluh Nopember (ITS), Surabaya, Indonesia, in 2015, where he is currently pursuing the Ph.D. degree. He is a Lecturer in energy engineering with the Department of Mechanical Engineering, Politeknik Negeri Ujung Pandang. His research interests include power system stability, renewable energy, and artificial intelligence.

WASEDA HIMAWARI was born in Japan, in January 2001. She received the bachelor's degree from the Department of Electrical Engineering, Institut Teknologi Sepuluh Nopember (ITS), Surabaya, Indonesia, in 2023, where she is currently pursuing the master's degree. Her research interests include the detection and identification of partial discharge types.